

Calculation of Gate Leakage Current in Deep Submicron MOSFET in the Presence of Electron Phase-breaking Scattering

by



Haif Uz Zaman

A Thesis submitted to
the Department of Electrical and Electronic Engineering of
Bangladesh University of Engineering and Technology, Dhaka
in partial fulfillment of the requirements
for the degree of
MASTER OF SCIENCE IN ELECTRICAL AND ELECTRONIC
ENGINEERING

DEPARTMENT OF ELECTRICAL AND ELECTRONIC ENGINEERING
BANGLADESH UNIVERSITY OF ENGINEERING AND TECHNOLOGY



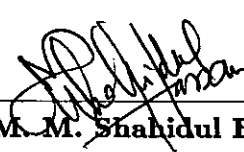
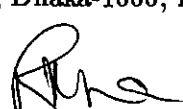
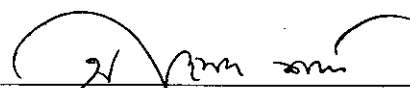
May 2001



#95184#

The thesis " Calculation of Gate leakage Current in Deep Submicron MOSFET in the Presence of Electron Phase-breaking Scattering" submitted by Saif Uz Zaman, Roll No. 9606244F, Registration No. 91197, Session 1995-96-97 to the Department of Electrical and Electronic Engineering, BUET has been accepted as satisfactory for partial fulfillment of the requirements for the degree of Master of Science in Engineering (Electrical and Electronic).

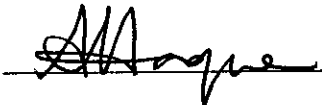
BOARD OF EXAMINERS

1.  14/5/2001
Dr. Anisul Haque Chairman
Associate Professor (Supervisor)
Department of Electrical and Electronic Engineering
BUET, Dhaka-1000, Bangladesh.
2.  14.5.2001
Dr. Shahidul Islam Khan Member
Professor and Head (Ex-officio)
Department of Electrical and Electronic Engineering
BUET, Dhaka-1000, Bangladesh.
4. 
Dr. M. M. Shahidul Hassan Member
Professor
Department of Electrical and Electronic Engineering
BUET, Dhaka-1000, Bangladesh.
3. 
Dr. M. Rezwan Khan Member
Professor
Department of Electrical and Electronic Engineering
BUET, Dhaka-1000, Bangladesh.
5. 
Dr. Ahmed Shafee Member
Professor (External)
Department of Physics
Dhaka University, Dhaka-1000, Bangladesh.

DECLARATION

It is hereby declared that this thesis or any part of it has not been submitted elsewhere for the award of any degree or diploma.

Signature of the supervisor



Dr. Anisul Haque

Associate Professor

Department of Electrical and Electronic Engineering

BUET, Dhaka 1000.

Signature of the candidate



Saif Uz Zaman

DEDICATION

To My Mother.

Contents

1	Introduction	1
1.1	Literature Review	2
1.2	Objective of the Work	6
1.3	Organization of the Thesis	7
2	Review of Quantum Mechanical Analysis of MOS Devices	8
2.1	Self-consistent Solution	8
2.2	Airy Function Technique	11
2.3	Variational Technique	12
3	Review of Transmission Line Analogy and Green's Function Formalism	13
3.1	Transmission Line Analogy	13
3.2	Green's Function Formalism	16
4	Direct Tunneling Current from Density-of-States	18
4.1	Theory	18
4.2	Results and Discussion	19
5	Direct Tunneling Current in the Presence of Scattering	37
5.1	Theory	37
5.2	Results and Discussions	40
6	Conclusion	52
6.1	Summary	52
6.2	Suggestions for Further Work	53
	Bibliography	54

List of Figures

2.1	A typical nMOS structure.	9
2.2	A typical conduction band profile for an nMOS structure.	9
3.1	A potential barrier with an incident electron (solid line) and the reflected wave(dashed line).	14
4.1	The empirical relationship between total band bending Φ_s and surface electric field F_S	21
4.2	Potential energy profile for two F_S	22
4.3	Variation of carrier concentration with F_S for a given t_{ox}	24
4.4	Variation of FWHM with eigenstate number for different t_{ox} and a given F_S	25
4.5	Variation of lifetime with eigenstate number for different t_{ox} and a given F_S	26
4.6	Variation of FWHM for the first three eigenstates with F_S for a given t_{ox}	27
4.7	Variation of lifetime of first three eigenstates with F_S for a given t_{ox}	28
4.8	Variation of DOS around the first three eigenenergies with energy for a given t_{ox} and F_S at checkpoint = 28 Å from the interface. $t_{ox}= 2$ nm, $F_S = 0.51$ MV/cm.	30

4.9	Variation of DOS around the first three eigenenergies with energy for a given t_{ox} and F_S at checkpoint = 55 Å from the interface. $t_{ox} = 2$ nm, $F_S = 0.51$ MV/cm.	31
4.10	Variation of contributions of first three eigenstates to gate leakage current with F_S for a given t_{ox}	32
4.11	Variation of 1st, 2nd, 3rd eigenenergy and Fermi energy with respect to bottom of the quantum well as functions of F_S for $t_{ox}=2$ nm.	33
4.12	Variation of gate leakage current with F_S for different t_{ox}	35
4.13	Variation of gate leakage current with V_g for different t_{ox}	36
5.1	Variation of B for lowest two eigenenergies for different t_{ox} . B1 corresponds to the lowest state and B2 corresponds to the second lowest state.	44
5.2	Variation of B for 1st eigenenergy for two different values of collision time and two different collision time profiles.	46
5.3	Variation of lifetimes of different eigenstates for two different values of collision time and two different collision time profile with $F_S = 0.51$ MV/cm and $t_{ox} = 2$ nm.	47
5.4	Variation of lifetimes of different eigenstates for two different values of collision time and two different collision time profile with $F_S = 1.66$ MV/cm and $t_{ox} = 2$ nm.	48
5.5	Variation total gate current with gate voltage with and without phase-breaking scattering for three t_{ox} , for constant $\tau_{coll} = 10^{-9}$ s.	49

5.6 Variation total gate current with gate voltage with and without phase-breaking scattering for three t_{ox} , for constant $\tau_{coll} = 10^{-10}$ s. 50

List of Tables

4.1	The values of eigenenergies in eV measured from the bottom of the potential well for three different surface electric fields, and gate oxide width, $t_{ox} = 2$ nm.	23
5.1	Relationship among calculated Γ_t , Γ_l and Γ_s for different eigenstates for $F_S = 0.51$ MV/cm, $\tau_{coll} = 10^{-9}$ s and $t_{ox} = 2$ nm. . .	41
5.2	Relationship among calculated Γ_t , Γ_l and Γ_s for different eigenstates for $F_S = 0.51$ MV/cm, $\tau_{coll} = 10^{-10}$ s and $t_{ox} = 2$ nm. . .	42
5.3	Relationship among calculated Γ_t , Γ_l and Γ_s for different eigenstates for $F_S = 3$ MV/cm, $\tau_{coll} = 10^{-9}$ s and $t_{ox} = 2$ nm. . . .	43
5.4	Relationship among calculated Γ_t , Γ_l and Γ_s for different eigenstates for $F_S = 3$ MV/cm, $\tau_{coll} = 10^{-10}$ s and $t_{ox} = 2$ nm. . . .	43
5.5	Comparison of the value of gate leakage current for exponential and constant profiles of τ_{coll} . $t_{ox} = 2$ nm.	45

ACKNOWLEDGEMENT

The author is deeply grateful to his supervisor Dr. Anisul Haque, Associate Professor, Dept. of EEE, BUET, for his continuous guidance, suggestions and wholehearted supervision in pursuing this work, without which this thesis never be materialized. The author has drawn upon the knowledge and expertise of Dr. Anisul Haque on every occasion in accomplishing the work. His patience and understanding is very much appreciated.

The author is grateful to Mr. Fayyaz Khan, Associate Professor and Head, Dept. of EEE, Ahsanullah University of Science and Technology (AUST), who provided with all the facilities of the department and cooperation to complete the work. In this regard, the author also likes to express thanks and gratitude to Dr. Shahidul Islam Khan, Professor and Head, Dept. of EEE, BUET.

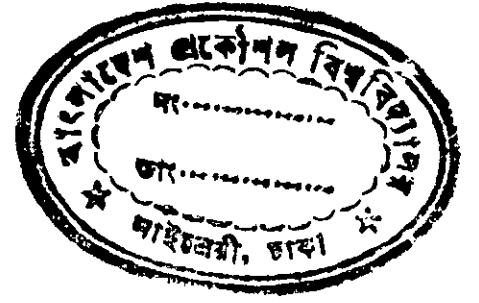
The author also expresses deep gratitude to Mr. Md. Iqbal Bahar Chowdhury, Lecturer, Dept. of EEE, AUST, for his invaluable software support and helpful advice. Also the author gratefully recalls the spontaneous inspiration obtained from Mr. Murshed Mahmud Chowdhury, Lecturer, Dept. of EEE, AUST.

Finally, the author would like to thank his brother and parents for their inspiration and encouragement throughout the progress of this work, which made the thesis a possible one.

ABSTRACT

When the gate length of a MOSFET enters into deep-submicron regime, Quantum Mechanical (QM) effects cannot be ignored. Quantization of inversion layer electrons increase effective gate oxide width, which, in turn, modifies the gate capacitance, threshold voltage, inversion charge density etc. In addition, a gate leakage current flows due to direct QM tunneling of electrons. This current has already been determined both experimentally and theoretically. The existing simulation techniques involve direct solution of Schrödinger's equation that results in complex eigenenergies and requires lengthy matrix manipulation. Moreover, it has been found that there is some discrepancy between the experimental and simulation results.

In this work, the direct tunneling gate current has been calculated using a simple technique which is easy to implement numerically. This method is based on Green's function formalism with transmission line analogy. Also, for the first time, the calculation of direct tunneling gate current incorporates the effects of electron phase-breaking scattering in the gate oxide. The current is calculated both ignoring and considering the effects of electron phase-breaking scattering. These results have been compared with the existing experimental and calculated values. The results found, proposes an explanation for the discrepancy between measured and existing simulated currents. It is concluded that it is necessary to include effects of phase-breaking scattering to accurately simulate direct tunneling gate leakage current.

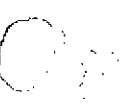


Chapter 1

Introduction

The advancement of the semiconductor device fabrication technology has grown very rapidly in last few years, consequently the aggressive scaling down of the same has taken place. It is expected that device length in nanometer range will be common in the near future. According to scaling rules, different dimensions (gate length, oxide width etc) of MOSFET are scaled down proportionately and the substrate doping concentration is increased. According to National Technological Roadmap for Semiconductors[1], for a device of gate length less than 100 nm, the oxide width should be less than 2.0 nm. For such deep submicron devices, when a strong Surface Electric Field (F_S) is present at the Si/SiO_2 interface, the energy band of silicon bends significantly, creating a quantum well. Due to quantization of energies of the inversion layer carriers in this quantum well, the distribution of carriers can no longer be represented by semi-classical models [2, 3], rather Quantum Mechanical (QM) model must be used. QM approach is essential for the calculation of several parameters; such as, gate capacitance, carrier concentration, effective oxide thickness, drive current, on-state series resistance, polysilicon work function, gate leakage current etc.

The potential barrier for inversion electrons at the Si/SiO_2 interface is finite and nearly equal to 3.1 eV. Since the width of the oxide layer is also finite, inversion electrons may tunnel through the oxide barrier and reach gate electrode. The tunneling probability is extremely small in conventional MOSFETs. But in deep submicron MOSFETs, with oxide width equal to 2 nm or less, the tunneling probability is high. Consequently a dc gate leakage current due to quantum mechanical tunneling flows in these devices.



1.1 Literature Review

The Quantum Mechanical (QM) effects in MOS inversion layers arise when high surface electric field makes the quantum well for inversion carriers very steep and narrow, such that the electron energies are quantized in the direction normal to the interface. A significant amount of research work has been conducted to understand and model QM effects in MOS devices. In this section, a partial review of these works is presented.

Stern first reported the quantum mechanical calculations for Silicon inversion layer [4], where he solved coupled Schrödinger's and Poisson's equations self-consistently. Later Moglestue determined the charge distribution for electrons and holes for {100}-oriented Si/SiO_2 interface, both for weak and strong inversion [5].

In their pioneering work, Dort *et al.* proposed a simple model for explaining measurements in the high doping level regime where the conventional model fails to reproduce the experimental results [6]. The model proposed by them uses the same drift-diffusion approximation used by semi-classical model [2], however some advanced physics is built in the simulators. This model modifies the intrinsic carrier concentration for the silicon bandgap inversion conditions. They showed that their model agreed with the results given by self-consistent QM calculation.

It is known that self-consistent solution of coupled Schrödinger's and Poisson's equations are numerically intensive and time consuming. Hareland *et al.* proposed a new computationally efficient model for predicting QM effects on the inversion layer charge density and charge distribution [7]. Their model utilizes analytical descriptions for the first three subbands of a 2-D density-of-states in a quantized electron inversion layer. This model, along with the one proposed by Dort *et al.* [6], has been implemented in a device simulator software named PISCES. These models show similar threshold voltage shifts, and effective oxide thickness' compared to classical simulation that use 3-D density-of-states at the interface.

Paasch *et al.* studied the effects of influence of inversion channel quantization on surface potential [8]. They showed that semi-classical description gives erroneous results while calculating surface potential or total band bending. They have shown that the error introduced in the calculation of surface potential is up

to some tenth volts with decreasing oxide width and increasing gate voltage.

Tagaki and Toriumi studied the inversion-layer capacitance of Si MOSFETs quantitatively [9]. The total gate capacitance, that determines the transconductance of MOSFET, is reduced due to the presence of inversion-layer capacitance (C_{inv}). It is a fundamental problem in deep submicron MOSFETs. C_{inv} depends on the surface orientation, which signifies the importance of QM effects on C_{inv} at room temperature.

Tagaki *et al.* have also analyzed the influence of C_{inv} on low voltage operation of scaled CMOSFET [10]. It is found that as the band bending is not scaled with a reduction of gate oxide width (t_{ox}), the band bending on Si substrate due to (C_{inv}) poses a significant limitation on scaling down of supply voltage.

Jallepalli *et al.* have analyzed the effects of hole quantization on p-MOS device characteristics, and electron quantization on n-MOS devices [11]. They have provided a compact analytical model to describe the threshold voltage shifts due to quantum effects as a function of gate oxide thickness and doping concentration. The threshold voltage shift is also dependent on temperature, which is illustrated by them. For a range of doping concentration, they have calculated the effective oxide thickness as a function of oxide field.

Ritcher, Hefner and Vogel have very recently compared the results of an extensive ensemble of the most advanced available QM capacitance-voltage simulators and analysis packages for a range of metal-oxide-semiconductor device parameters [12]. They found that, for different simulators, in the accumulation capacitance region, extracted equivalent oxide thickness (EOT) shows on the order of 0.2 nm variations for total SiO_2 thickness in the range of 1.0 to 3.0 nm. Their study emphasizes on the fact that, when reporting experimentally derived electrical thickness results, it is essential to describe fully how these values were obtained. The same experimental curve can lead to different extracted EOT depending upon which Quantum Mechanical software is used for the analysis.

Giannini *et al.* have compared the results of measurements of MOS interface states by capacitance-voltage (C-V) and charge pumping techniques [13]. They have shown that, if the effects of carrier tunneling in slow oxide traps are not incorporated, the information on energy distribution of interface states given by both capacitance-voltage and charge pumping techniques will be erroneous.

It was commonly believed that QM effects were dominant only in strong in-

version conditions. However, Pacelli *et al.* have shown that semi-classical model of heavily doped MOSFETs is not valid even near flat band region [14]. The study of Pacelli *et al.* shows that even for a small vertical electric field, due to the presence of abrupt discontinuity, at the Si/SiO₂ interface, a “dark space” of a few nanometer results. In this “dark space”, the majority carrier density is much lower than in the bulk. Their work shows that even for a weak confining potential the QM effects prevails.

Barlage *et al.* have used the transmission line model for the MOSFET channel region for extraction of MOS inversion capacitance [15]. Their work corrects the capacitance measurement error introduced from high gate dielectric leakage in the inversion regime. Their approach incorporates accurately the leakage current distribution along the channel and produces a gate length dependent correction factor for the measured capacitance. This result overcomes the discrepancies that arose in the previously reported results using discrete element based model.

Fiegna and Abramo have analyzed the QM effects on gate capacitance, threshold voltages and effective mobility of electrons in nonuniformly doped MOS structures [16]. Their results show that, with the introduction of a low doped region at the device surface, it is possible to manipulate the threshold voltage according to the circuit application. Also for a given charge sheet density, the introduction of low doped epitaxial region produces a reduction of the electron effective field, resulting in the improvement of electron effective mobility. But it leaves the total gate capacitance unaffected.

An important aspect in the study of submicron MOSFETs is the calculation of gate leakage current due to direct tunneling. Rana *et al.* used self-consistent solutions of accumulation layers in n-substrate MOSFETs to calculate the tunneling current [17]. They used finite element method for the purpose. Tunneling current for inversion layer was studied by Lo *et al.* [18]. In this paper, they have mentioned that for the purpose of modeling tunneling characteristics of electrons, exhibiting quasi two-dimensional character, the transmission probability applicable to an incident Fermi gas of free electron is no more an acceptable concept and the well known WKB (Wentzel-Krammer-Brioullion) approximation or the numerical integration of Airy function is not valid. They have used the transverse resonant method, applicable for electromagnetic waves in a non-uniform waveguide, for solving the Schrödinger's equation. The complex eigenenergy found from

the solution of the equation is used to calculate the gate leakage current.

Taur has compared simulated and experimental results for MOSFETs having oxide thickness 2.2-3.5 nm [19]. Shih *et al.* have compared the leakage current found from the numerical solution to that found by using WKB approximation [20]. For the analysis, they have used Al as gate electrode. They had to find the complex eigenenergy of a non-Hermitian matrix. Their finding is that the gate leakage current found from the WKB approximation shows poor agreement at high gate voltages.

A modified WKB approximation has been proposed by Register *et al.* [21]. It modifies the usual tunneling probability predicted by WKB, by accounting the reflections from potential discontinuity. In this model, the barrier height to tunneling is taken to be a function only of the total electron energy and the Si bandgap dispersion relation is modeled as a two band Franz-type. Yang *et al.* have used this modified WKB approximation model for the calculation of the tunneling current [22]. However, for the self-consistent loop, the barrier at the Si/SiO₂ interface has been assumed to be infinite. Yang *et al.* have also studied the effects of variation of doping concentration of both substrate and polysilicon and observed the effects on gate leakage current. The suggestion that comes from their study is, alternative dielectric with higher dielectric constant may be used in lieu of SiO₂.

In order to have a greater understanding of how a dielectric stack with higher dielectric constant would effect the direct tunneling current, Mudanai *et al* have done some studies [23]. They have performed the numerical solution of Schrödinger's equation allowing wavefunction penetration into the gate dielectric stack. They have adopted a first order perturbation technique to incorporate wavefunction penetration effects into gate dielectric. This technique requires determination of complex eigenenergies of a non-Hermitian Hamiltonian. Since this is numerically a very time consuming technique, the wavefunction penetration effects were neglected in the self-consistent loop and incorporated only after convergence of the self-consistent loop assuming infinite barrier. If gate dielectric of high dielectric constant is used, certain problems, such as, fringing induced barrier lowering, may come into play.

Direct tunneling gate leakage current in devices with silicon nitride gate dielectric for both n and p MOSFETs has been studied by Yeo *et al.* [24]. They

have highlighted the important difference between silicon nitride and silicon dioxide. They have projected that jet-vapor deposition Si_3N_4 gate dielectric can be scaled down to 0.65 nm and 1.13 nm for high performance and low power application, respectively.

1.2 Objective of the Work

Self-consistent solution of Schrödinger's and Poisson's equations are usually used to determine quantum effects in Si inversion layers. Commonly used two boundary conditions for the solution of Schrödinger's equation are that the wavefunction goes to zero at Si/SiO_2 interface and at deep inside the bulk Si [4]-[11], [14, 16, 18, 20, 22]. When these boundary conditions are used, the effects of wavefunction penetration into the gate oxide, which is the cause of direct tunneling, on potential profile cannot be incorporated. To overcome this problem, Rana *et al.* have imposed an artificial boundary condition in their finite element analysis that the wavefunction is zero at oxide-gate electrode interface and at a finite distance inside the bulk semiconductor [17]. However, this led to problems of artificial charge pile up in bulk Si in their calculations. Others have bypassed this problem in two steps [18, 20, 22, 23]. First, they calculated the self-consistent potential profile neglecting the effects of wavefunction penetration into the oxide. This potential profile was then used to find the direct tunneling current in a postprocessor. The techniques used to calculate the direct tunneling current are either approximate [17, 22] or requires numerical determination of complex eigenenergies of a non-Hermitian matrix [18, 20, 23]. Recently, Mudanai *et al.* have done some preliminary studies on the effects of wavefunction penetration on self-consistent potential profile [23]. Without providing adequate justification, they have claimed that these effects are negligible while different studies indicate otherwise [25]. Moreover, their technique is numerically too time consuming to be used widely.

Another feature that has received almost no attention in the literature is the effects of electron inelastic scattering in gate-oxide on direct tunneling current. Due to the presence of phonons, defects and interface states in oxides, inversion electrons are known to experience phase-breaking scattering [26]-[30]. This scattering is expected to modify the lifetimes of quasi-bound inversion layer electrons

and change the gate leakage current.

In the present work, a new technique is presented to calculate direct tunneling gate current in MOSFETs with ultra-thin gate oxides. In this technique, new boundary conditions are used to solve Schrödinger's equation, which incorporates the effects of wavefunction penetration into the oxide. This technique is numerically efficient and does not require lengthy matrix manipulations. Phase-breaking scattering of electrons are also modeled in a straight forward manner. For the first time, influence of electron phase-breaking scattering on direct tunneling are studied. Numerical calculations based on this new technique are performed and results are compared to those of existing experimental and simulation studies.

1.3 Organization of the Thesis

Chapter 2 reviews quantum effects in MOS devices. Chapter 3 discusses the transmission line analogy and Green's function formalism. Chapter 4 narrates calculation of gate leakage current from the density-of-states. Here the current calculation is done without incorporating phase-breaking/inelastic scattering. Chapter 5 consists of the theory and results of the gate leakage current in the presence of phase-breaking scattering of electrons in the oxide. Concluding remarks of this work will be presented in chapter 6.

Chapter 2

Review of Quantum Mechanical Analysis of MOS Devices

Quantum effects in MOSFETs arise when the quantization of the inversion layer carriers occur due to the presence of a high electric field (F_S) at the surface of the semiconductor. In this chapter, a few approaches to the quantum mechanical analysis of the MOS structures are reviewed. The Structure of an n channel enhancement type MOS is seen in the Fig. 2.1.

2.1 Self-consistent Solution

The self consistent solution of coupled Schrödinger's and Poisson's equations as proposed by Stern [4] is presented in this section.

The three major approximations that Stern made are;

(i) Effective mass approximation is valid, so that the periodic lattice potential need not be taken into account explicitly.

(ii) Envelope wavefunction vanishes at the surface.

(iii) Surface states are neglected and any charge in the oxide adjacent to the semiconductor is replaced by an equivalent electric field. A typical conduction band profile for an nMOS structure is shown in Fig. 2.2

The band bending of a semiconductor can be characterized by a potential $\Phi(z)$. In the effective mass approximation, the electronic wavefunction for the i th subband is the product of the Bloch function at the bottom of the conduction band and the envelope function.

$$\psi_i(x, y, z) = \zeta_i(z) e^{i\theta z} e^{ik_1 x + ik_2 y}, \quad (2.1)$$

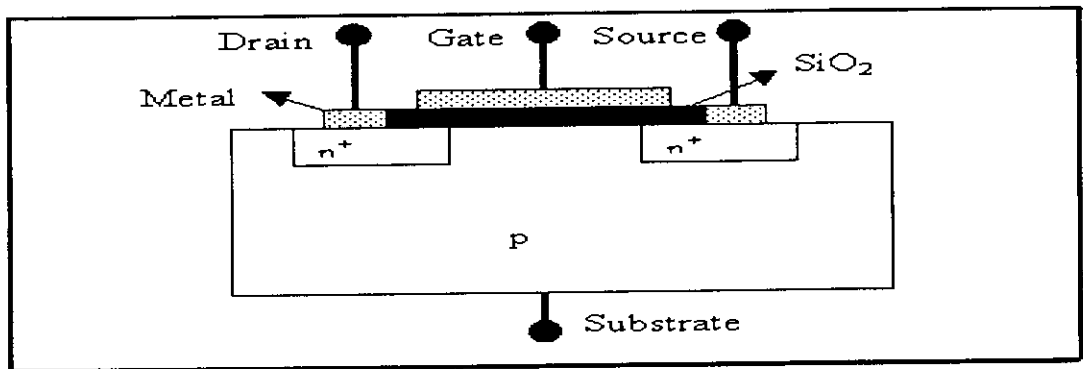


Fig. 2.1: A typical nMOS structure.

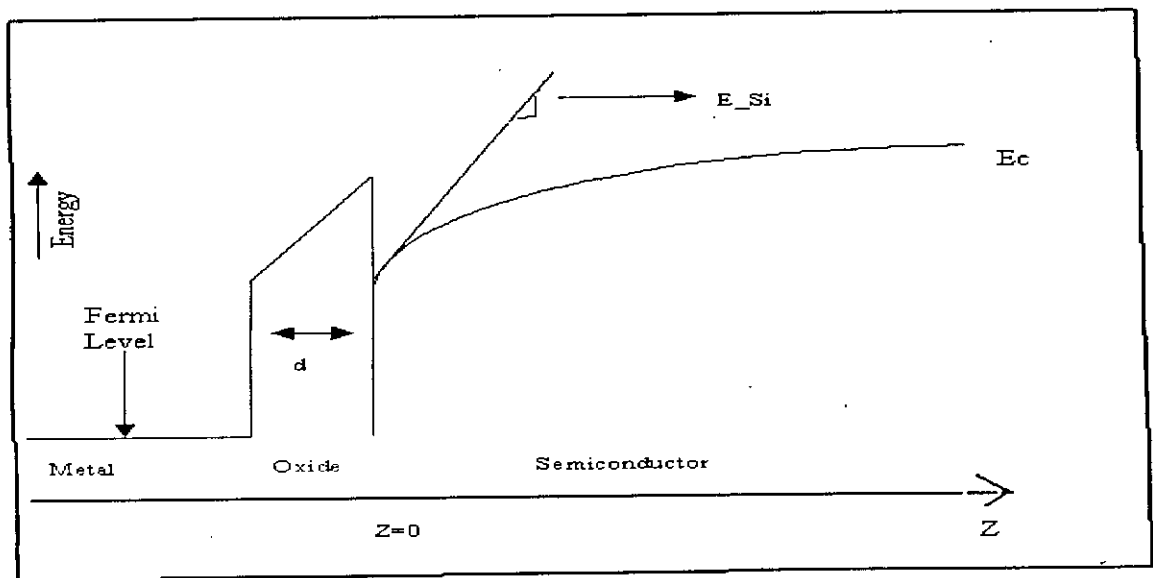


Fig. 2.2: A typical conduction band profile for an nMOS structure.

here, k_1 and k_2 are measured relative to the band edge, θ depends on k_1, k_2 . Envelope function $\zeta_i(z)$ is the solution of

$$\frac{d^2\zeta_i}{dz^2} + \frac{2m_3}{\hbar^2}[E_i + e\Phi(z)]\zeta_i(z) = 0. \quad (2.2)$$

Here, m_3 is the effective mass in the direction perpendicular to the interface and E_i is the energy of the i th bound state in the same direction. Boundary conditions commonly used for the solution of Eq. (2.2) are $\zeta_i(\infty) = 0$ and at the semiconductor-oxide interface, $\zeta_i(z = 0) = 0$. Each solution of Eq. (2.2) gives the bottom of a continuum of levels called a subband. A subband is described by the relationship,

$$E_{tot}(\vec{k}_{\parallel}) = E_i + \frac{\hbar^2 k_1^2}{2m_1} + \frac{\hbar^2 k_2^2}{2m_2}, \quad (2.3)$$

here, m_1 and m_2 are the principal effective masses for motion parallel to the surface and $\vec{k}_{\parallel} = k_1\hat{x} + k_2\hat{y}$. There can be as many as three values of m_3 depending on the surface orientation because the conduction band of Si has six ellipsoid valleys along the $\langle 100 \rangle$ family of direction. In the effective mass approximation, the valleys are degenerate in pairs. Solution of Eq. (2.2) gives the eigenenergy E_i and the envelope function $\zeta_i(z)$.

The potential $\Phi(z)$ is found from the solution of Poisson's equation, which is as follows,

$$\frac{d^2\Phi(z)}{dz^2} = -\frac{[\rho_{depl}(z) - e\sum_i N_i \zeta_i^2(z)]}{\epsilon_{si}\epsilon_o}, \quad (2.4)$$

here, ϵ_{si} is the dielectric constant of the semiconductor, N_i is the carrier concentration in the i th subband. N_i is given by the following equation,

$$N_i = \frac{n_{vi}m_{di}kT}{\pi\hbar^2} \ln \left[1 + \exp \left(\frac{E_F - E_i}{kT} \right) \right], \quad (2.5)$$

where, n_{vi} is the valley degeneracy of i th valley, m_{di} is the density-of-states effective mass per valley and E_F is the Fermi energy.

$\rho_{depl}(z)$ is the charge density in the depletion layer, which is taken to be,

$$\rho_{depl}(z) = -e(N_A - N_D), \quad 0 < z < z_d \quad (2.6)$$

$$\rho_{depl}(z) = 0, \quad z > z_d \quad (2.7)$$

here, z_d is the depletion layer thickness given by [4] as following,

$$z_d = \sqrt{\frac{2\epsilon_{si}\epsilon_o\Phi_d}{e(N_A - N_D)}}. \quad (2.8)$$

Φ_d is the band bending due to depletion charge only. Φ_d can be calculated from [4] as following,

$$\Phi_d = \Phi_s - \frac{kT}{e} - \frac{eN_{inv}z_{av}}{\epsilon_{si}\epsilon_o}. \quad (2.9)$$

Where $N_{inv} = \sum_i N_i$ is the total number of charge per unit area in the inversion layer and z_{av} is the average penetration of inversion charge density into Si . The two boundary conditions for solution of Eq. (2.4) are $\frac{d\phi}{dz} = 0$ for large z and at the surface, its value is F_S . From [4], F_S is given by,

$$F_S = \frac{e(N_{inv} + N_{depl})}{\epsilon_{si}\epsilon_o}. \quad (2.10)$$

$N_{depl} = z_d(N_A - N_D)$ is the number of charge per unit area in the depletion layer. In a self-consistent formulation, Eqs. (2.2)-(2.9) are solved iteratively for a given F_S until results converge.

2.2 Airy Function Technique

For the purpose of finding self-consistent solution of Schrödinger's and Poisson's equations, it is necessary to solve them numerically. However, approximate results can be obtained for some simple limiting cases.

A triangular potential approximation can be done by replacing the potential $\Phi(z)$, in Eq. (2.2), by assuming $\Phi(z) = -zF_S$ for $z > 0$ and $\Phi(z) \rightarrow \infty$ for $z < 0$. Analytical solution for this potential profile gives what is known as Airy functions Ai from [4]:

$$\zeta_i(z) = Ai \left(\left(\frac{2m_3eF_S}{\hbar^2} \right)^{\frac{1}{3}} \left[z - \left(\frac{E_i}{eF_S} \right) \right] \right), \quad (2.11)$$

$$E_i \approx \left(\frac{\hbar^2}{2m_3} \right)^{\frac{1}{3}} \left[\frac{2}{3}\pi eF_S \left(i + \frac{3}{4} \right) \right]^{\frac{2}{3}}. \quad (2.12)$$

2.3 Variational Technique

Triangular potential approximation fails when the inversion layer charge density is comparable to or exceeds that of the depletion layer. When only one subband is occupied, i.e., in the electric quantum limit, a Variational approach gives a good estimate for the energy of the lowest subband. A trial eigenfunction given in Eq. (2.13) is

$$\zeta_o(z) = \left(\frac{1}{2}b^3\right)^{\frac{1}{2}} z e^{-\frac{bz}{2}}. \quad (2.13)$$

Here b is an unknown parameter. After some straight forward calculation, the energy of the lowest state is as follows,

$$E_o = \frac{\hbar^2 b^2}{8m_3} + \left(\frac{3e^2}{\epsilon_{si}\epsilon_o b}\right) \times \left[N_{depl} + \frac{11}{16}N_{inv} - \frac{2}{b}(N_A - N_D)\right]. \quad (2.14)$$

The term involving N_{inv} gives the interaction of inversion-layer charge density with itself. The correct choice of b minimizes the total energy of the system, in which the coefficient $\frac{11}{16}$ is replaced by $\frac{11}{32}$. The last term of the Eq. (2.14) is small for Si, as in Si the width of the inversion layer is generally much smaller than that of the depletion layer.

Chapter 3

Review of Transmission Line Analogy and Green's Function Formalism

Numerical determination of eigenenergies and wavefunctions from Schrödinger's equation for an arbitrary potential profile is complicated and often requires lengthy matrix manipulation. In this chapter, a simple technique based on transmission line analogy for calculation of eigenenergies is presented. This technique is then extended using Green's function formalism to find the wavefunctions and local density-of-states (DOS).

3.1 Transmission Line Analogy

Microwave transmission line theory can be used for solving problems related to quantum mechanical wave as shown in [30]. The familiar equations for voltage and current in transmission line are [31],

$$I(z) = I^+(e^{\gamma_r z} - \Gamma_t e^{-\gamma_r z}), \quad (3.1)$$

$$V(z) = I^+ Z_0 (e^{\gamma_r z} + \Gamma_t e^{-\gamma_r z}). \quad (3.2)$$

Here I^+ is the amplitude of incident current wave and γ_r is the propagation constant. The time dependence is implicitly assumed to be $e^{-j\omega t}$. The wave amplitude reflection coefficient Γ_t is given by

$$\Gamma_t = \frac{Z_{it} - Z_{ot}}{Z_{it} + Z_{ot}}. \quad (3.3)$$

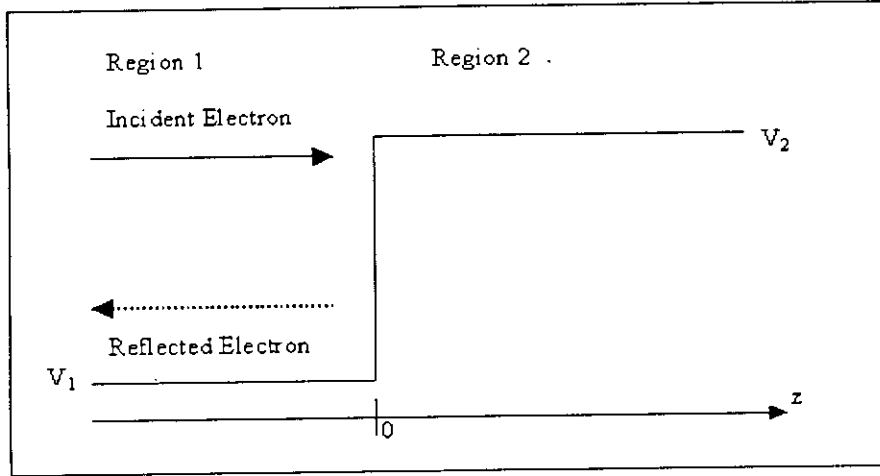


Fig. 3.1: A potential barrier with an incident electron (solid line) and the reflected wave(dashed line).

Here Z_{it} and Z_{ot} are the load and characteristic impedance, respectively.

Let us now consider solution of Schrödinger's equation. In Fig. 3.1 a traveling wave is incident on a potential barrier from the left. Energy of the electron is E . The wavefunction ψ can be written as

$$\psi_i(z) = A^+(e^{\gamma_i z} - \rho e^{-\gamma_i z}), \quad (3.4)$$

$e^{-jEt/\hbar}$ is implicitly assumed to be the time dependence of the wavefunction. Here

$$\gamma_i = \alpha_i + j\beta_i = j\sqrt{\frac{2m_i^*}{\hbar^2}(E - V_i)}, \quad (3.5)$$

is the propagation constant, m_i^* and V_i are effective mass and potential for the i th ($i = 1, 2$) region in Fig. 3.1, respectively and ρ is the wave amplitude reflection coefficient.

When $i = 1$ ($z < 0$), the wavefunction is,

$$\psi_1(z) = A_1^+(e^{\gamma_1 z} - \rho e^{-\gamma_1 z}), \quad (3.6)$$

when $i = 2$ ($z > 0$), the wavefunction is

$$\psi_2(z) = A_2^+ e^{\gamma_2 z}. \quad (3.7)$$

Now, the two boundary conditions, that the wavefunction and its derivative must be continuous at $z = 0$, gives the expression for ρ as

$$\rho = \frac{\frac{\gamma_2}{m_2^*} - \frac{\gamma_1}{m_1^*}}{\frac{\gamma_2}{m_2^*} + \frac{\gamma_1}{m_1^*}}. \quad (3.8)$$

Let,

$$\phi(z) = \frac{2\hbar}{jm^*} \frac{d\psi}{dz}, \quad (3.9)$$

then,

$$\phi(z) = A^+ Z_0 (e^{\gamma z} + \rho e^{-\gamma z}), \quad (3.10)$$

where,

$$Z_0 = \frac{2\gamma\hbar}{jm^*}. \quad (3.11)$$

Using this expression of Z_0 in Eq.(3.8), it is found that

$$\rho = \frac{Z_{0,2} - Z_{0,1}}{Z_{0,2} + Z_{0,1}}. \quad (3.12)$$

where, $Z_{0,1}$ and $Z_{0,2}$ are defined for region 1 and region 2, respectively. Comparing Eq. (3.1) with Eq. (3.4) and Eq. (3.2) with Eq. (3.10) and, Eq. (3.3) with Eq. (3.12) the analogy between $I(z)$ and $\psi(z)$, $\phi(z)$ and $V(z)$, Γ_t and ρ can be established. At any point z , the quantum mechanical wave impedance is defined as

$$Z(z) = \frac{\phi(z)}{\psi(z)}. \quad (3.13)$$

Thus, transmission line theory can be applied for QM calculations. For example, the input impedance, Z_i at $z = -l$ may be expressed in terms of load impedance, Z_l at $z = 0$ as in transmission line theory. Using Eq. (3.4) and Eq. (3.10) in Eq. (3.13) [31]

$$Z_i = Z_0 \frac{Z_l \cosh(\gamma l) - Z_0 \sinh(\gamma l)}{Z_0 \cosh(\gamma l) - Z_l \sinh(\gamma l)}. \quad (3.14)$$

Eigenenergies of arbitrary quantum wells can also be determined using quantum mechanical impedance. At any eigenenergy, the wave impedances looking to the right (positive direction) and to the left (negative direction), at any plane z inside the well, must be equal, i.e.

$$Z_{iR} = Z_{iL}, \quad (3.15)$$

here, subscript R and L refer to the impedance looking to the right and left, respectively.

3.2 Green's Function Formalism

The Green's function is used to calculate the wavefunction and the DOS as shown in [32]. The logarithmic derivative of the retarded Green's function is defined by,

$$Z(z, z'; E) = \frac{2\hbar}{jm^*} \left[\frac{\partial G^R(z, z'; E)}{\partial z} / G^R(z, z'; E) \right]. \quad (3.16)$$

Here, G^R is the retarded Green's function that satisfies the following equation.

$$\left[E + \frac{\hbar^2}{2m^*} \frac{\partial^2}{\partial z^2} - V(z) + i\epsilon \right] G^R(z, z'; E) = \delta(z - z'), \quad (3.17)$$

where, ϵ is an infinitesimally small positive energy. Owing to the nature of G^R , $Z(z, z'; E)$ has a discontinuity at $z = z'$. It can be shown that $Z(z, z'; E)$ does not depend on z' as long as $z > z'$ ($z < z'$) [32]. i.e,

$$Z(z, z'; E) = Z_{iR}(z; E) \quad \text{for all } z' < z \quad (3.18)$$

$$Z(z, z'; E) = Z_{iL}(z; E) \quad \text{for all } z' > z. \quad (3.19)$$

$Z_{iR}(Z_{iL})$ for a given energy can be calculated as functions of positions assuming that the potential profile is flat in both directions sufficiently far from the region of interest. This leads to the following two boundary conditions. The boundary conditions for calculating Z are $Z_{iR}(\infty; E) = Z_o(\infty)$ and $Z_{iL}(-\infty; E) = -Z_o(-\infty)$, where

$$Z_o = \frac{2\hbar}{jm^*} \gamma(z), \quad (3.20)$$

and

$$\gamma(z) = j \left(\frac{2m^*}{\hbar^2} [E - V(z) + j\epsilon] \right)^{1/2}. \quad (3.21)$$

Using the transmission line analogy the eigenenergies can be located, and then the normalized wavefunction is obtained from the diagonal part of G^R [32].

$$|\psi_n(z)|^2 = -\epsilon \Im m [G^R(z, z; E_n)], \quad (3.22)$$

where, E_n is the eigenenergy corresponding to the n th wavefunction. Using Eqs. (3.16), (3.17), (3.18) and (3.19), Eq. (3.22) can be expressed as

$$|\psi_n(z)|^2 = \frac{4\epsilon}{\hbar} \Im m \left[\frac{j}{Z_{iR}(z; E_n) - Z_{iL}(z; E_n)} \right]. \quad (3.23)$$

By definition, the one dimensional (1D) DOS is also given by the imaginary part of the diagonal term of 1D retarded Green's function G^R

$$N(z; E) = -\frac{1}{\pi} \Im m[G^R(z, z; E)]. \quad (3.24)$$

Relating diagonal part of G^R to quantum mechanical impedance, Eq. (3.24) reduces to,

$$N(z; E) = \frac{4}{\pi \hbar} \Im m \left[\frac{j}{Z_{iR}(z; E_n) - Z_{iL}(z; E_n)} \right]. \quad (3.25)$$

Chapter 4

Direct Tunneling Current from Density-of-States

Inversion electrons can tunnel into gate electrode from Si inversion layers as the height and width of the oxide barrier is finite. The tunneling probability increases exponentially with reduction of gate-oxide thickness. As a consequence of tunneling, a leakage current flows in the gate. Due to the leakage, the lifetime of inversion carriers become finite and the DOS broadens in energy around the eigenvalues.

4.1 Theory

The gate current due to quantum mechanical (QM) tunneling is calculated from the carrier concentration and the lifetimes of the carriers at all eigenstates using following relationship [18],

$$J = \sum_i \frac{eN_i}{\tau_i}. \quad (4.1)$$

Here, N_i is the concentration of the electrons in the i th eigenstate, τ_i is the lifetime of the electrons in the i th eigenstate and J is the total gate leakage current. The carrier concentration due to i th eigenstate from [4] is given by Eq. (2.5). Typically, eigenenergy E_i and concentration N_i are calculated numerically from the solutions of Schrödinger's equation for bound systems [18, 20]. In the presence of leakage, the Hamiltonian for a closed system becomes non-Hermitian and the eigenenergies become complex. The real parts give the energies of the quasi-bound states and the imaginary parts are related to the lifetimes. Since calculation of complex

eigenenergies is numerically complicated, a simple alternate technique is used in this work. The DOS is known to broaden in energy in systems with quasi-bound states. The peak of the DOS occurs at the eigenenergies of the quasi bound states and the lifetimes of the inversion layer electrons are related to the energy broadening of DOS according to,

$$\tau_i = \frac{\hbar}{2\Gamma_i}. \quad (4.2)$$

Here, Γ_i is the Full-Width at Half-Maximum (FWHM) of the energy broadening around the i th eigenenergy. The position dependent DOS as a function of energy around each eigenenergy is calculated using Eq. (3.24). The FWHM of the DOS can be evaluated anywhere inside the well since it has been shown earlier that the energy broadening of the DOS is the same at all positions [33]. The gate leakage current can easily be calculated from Eqs. (2.5), (4.1) and (4.2).

It may be mentioned that the inversion layer potential profile and the total band bending depend on the applied gate voltage, which, in turn, depends on F_S , the surface electric field at the Si/SiO_2 interface. The gate voltage (V_g) is related to F_S by the equation

$$V_g = \Phi_s + t_{ox}F_{ox} + \Phi_{ms} + d_mF_S, \quad (4.3)$$

here, t_{ox} is the physical gate oxide width, $F_{ox} = \epsilon_{Si}F_S/\epsilon_{ox}$ is the electric field in the oxide, Φ_s is the total band bending, Φ_{ms} is the difference between ‘metal’ and semiconductor workfunctions and d_m is the polysilicon depletion width. Here gate electrode has been taken to be heavily doped polysilicon.

4.2 Results and Discussion

The analysis has been done for {111} Si at room temperature. Results of numerical calculations for nMOS structures are presented in this section. The substrate doping density, $N_a = 5 \times 10^{17} /cm^3$.

Ideally the potential profile should be determined from self-consistent solution of Schrödinger’s and Poisson’s equations. However, for the sake of simplicity, self-consistent calculation is avoided. The potential profile has been assumed to be exponential and the relationship between surface electric field, F_S and band

bending Φ_s is described by an empirical formula that agrees well with the self-consistent results reported in [34]. The formula is as following,

$$F_S = k\Phi_s^5, \quad (4.4)$$

where, k is an arbitrary constant. The dependence of Φ_s with F_S is shown in Fig. 4.1.

The conduction energy band diagram for the MOS inversion layer for two F_S is shown in Fig. 4.2. The conduction band minima in polysilicon gate is chosen as the reference of the zero energy. With the increase of F_S , the total band bending (Φ_s) increases and the potential well gets steeper. As the potential well gets steeper, the number of eigenstates decreases, as well as, the value of any eigenenergy increases. Table 4.1 shows the values of the eigenenergies for three F_S and $t_{ox} = 2$ nm.

The total concentration of electrons ($N_{inv} = \sum_i N_i$) in the inversion layer increases almost exponentially with the increase of F_S , as seen in the Fig. 4.3. This variation is expected, as from Eq. (2.5), it is seen that the concentration increases with the increase of the difference of Fermi energy and the values of the eigenenergies. This difference increases with the increase of the F_S .

Fig. 4.4 shows the variation of FWHM with the number of eigenstates for a certain F_S and three different t_{ox} . For any eigenstate, the FWHM (which signifies the broadening) increases exponentially with the decrease of t_{ox} for a given F_S . It means that, the tunneling probability increases as the gate oxide width decreases. Another feature of merit is that, the FWHM does not increase monotonically with increasing number of eigenstates for a given t_{ox} and F_S . It increases for the first few eigenstates, then starts to decrease. A qualitative explanation for this unusual behaviour is given in [33]. As expected, the behaviour of τ_i is opposite to that of Γ_i . The lifetime is related with the FWHM by Eq. (4.2). Fig. 4.5 shows the decreasing nature of lifetime of electrons in any eigenstate with decrease of t_{ox} for a given F_S .

Fig. 4.6 shows the variation of FWHM for first three eigenstates with F_S for a given t_{ox} . It is seen that the broadening of any eigenstate, or the tunneling transparency of the barrier increases nearly exponentially with the increase of F_S . Also, as Fig. 4.7 shows, with increase of F_S , the lifetime decreases exponentially. At lower fields, the lifetimes of all three states have similar values, but at higher

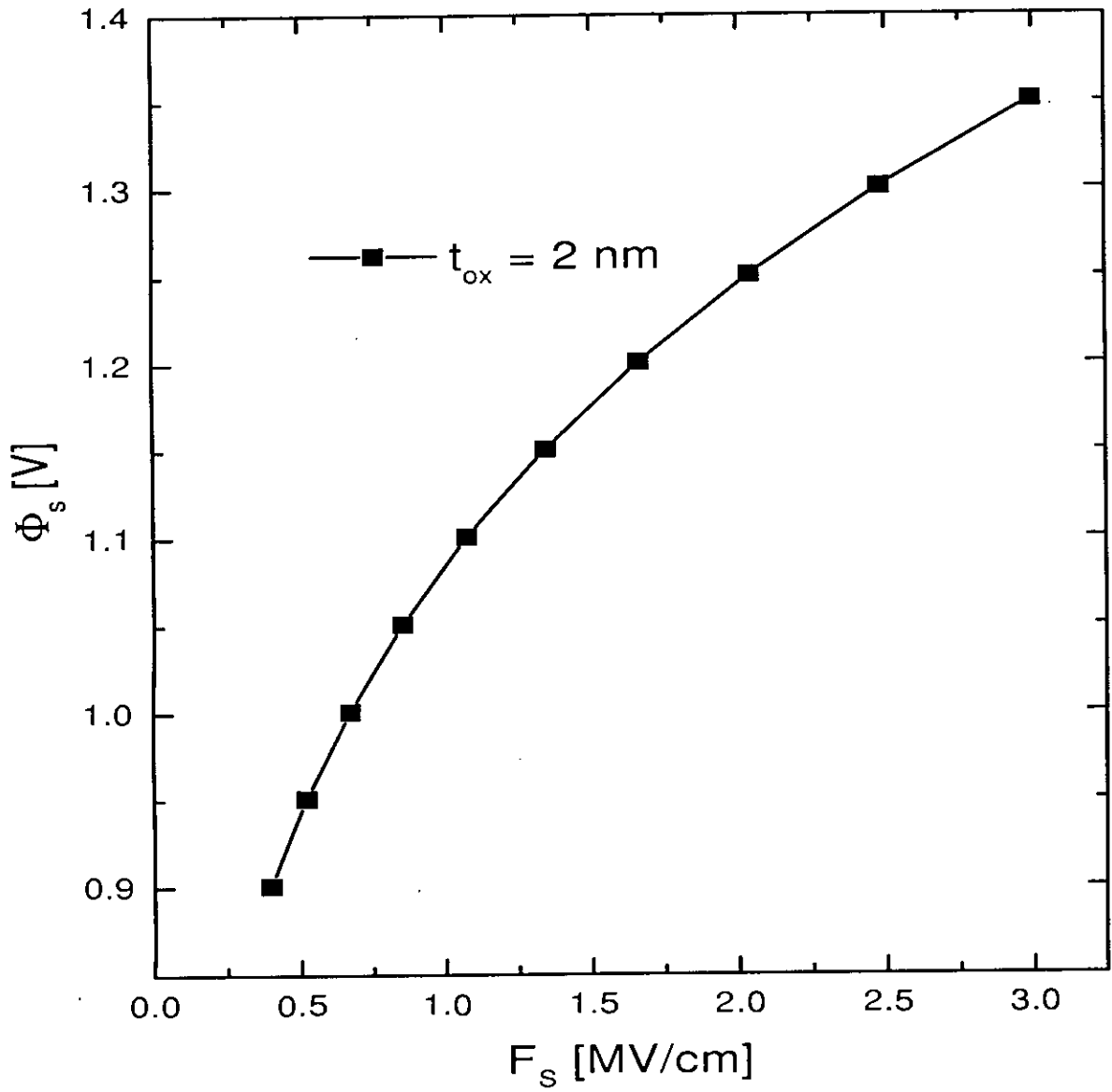


Fig. 4.1: The empirical relationship between total band bending Φ_s and surface electric field F_s .

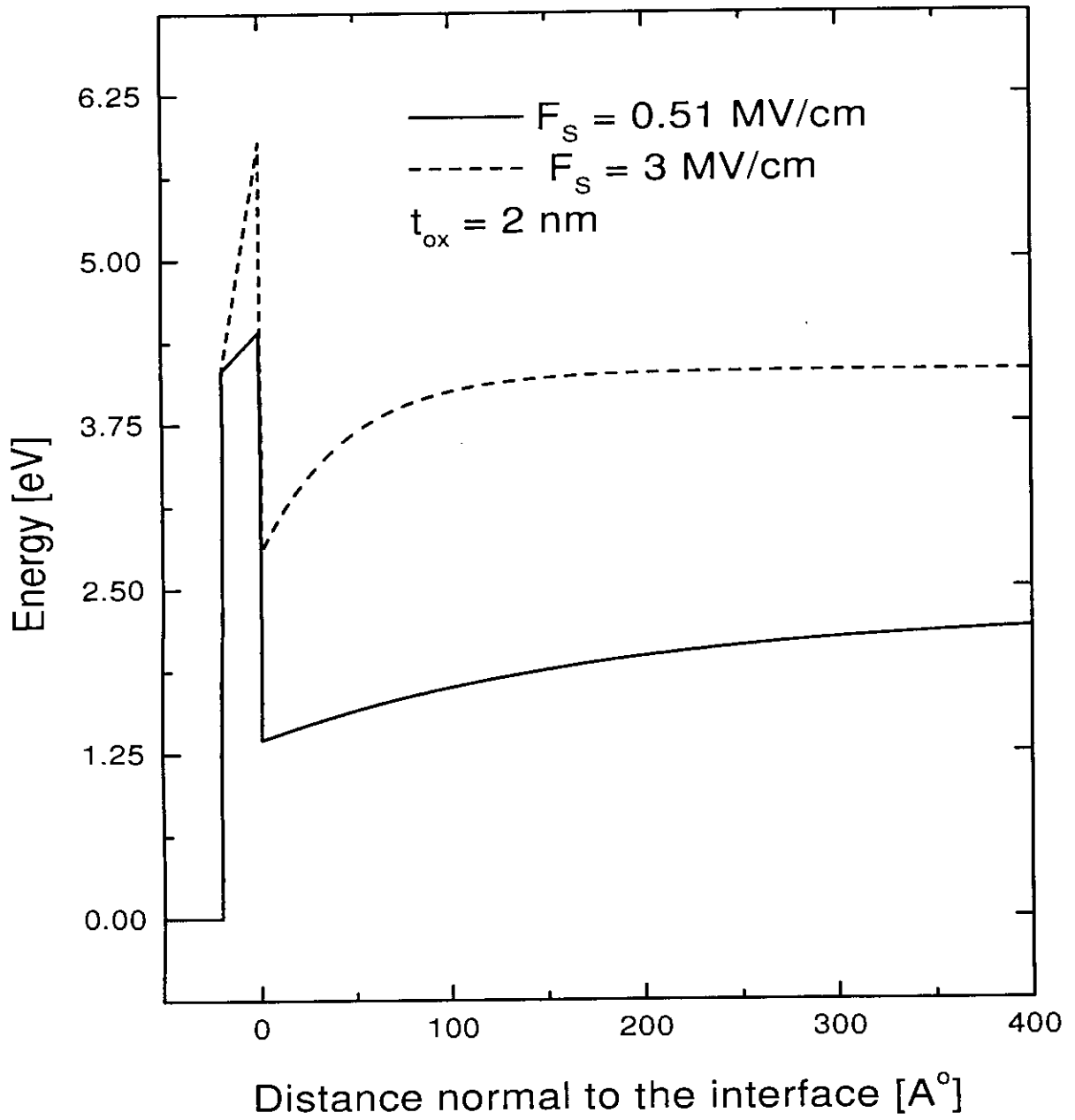


Fig. 4.2: Potential energy profile for two F_S .

Eigen- number	$F_S = 0.50$ (MV/cm)	$F_S = 1.07$ (MV/cm)	$F_S = 3.00$ (MV/cm)
1	0.151235	0.236237	0.43054
2	0.264077	0.410502	0.737405
3	0.349723	0.537857	0.940681
4	0.420419	0.639105	1.085279
5	0.480979	0.722499	1.189329
6	0.533945	0.792432	1.262625
7	0.580877	0.851616	1.311296
8	0.622822	0.901886	1.339545
9	0.660529	0.944562	-
10	0.694561	0.980639	-
11	0.725354	1.010894	-
12	0.753254	1.035949	-
13	0.778546	1.056313	-
14	0.801463	1.072412	-
15	0.822206	1.084607	-
16	0.840942	1.093206	-
17	0.857819	1.098478	-
18	0.872964	-	-
19	0.886489	-	-
20	0.898494	-	-
21	0.909068	-	-
22	0.918291	-	-
23	0.926234	-	-
24	0.932965	-	-
25	0.938541	-	-
26	0.943019	-	-
27	0.946449	-	-
28	0.948876	-	-

Table 4.1: The values of eigenenergies in eV measured from the bottom of the potential well for three different surface electric fields, and gate oxide width, $t_{ox} = 2$ nm.

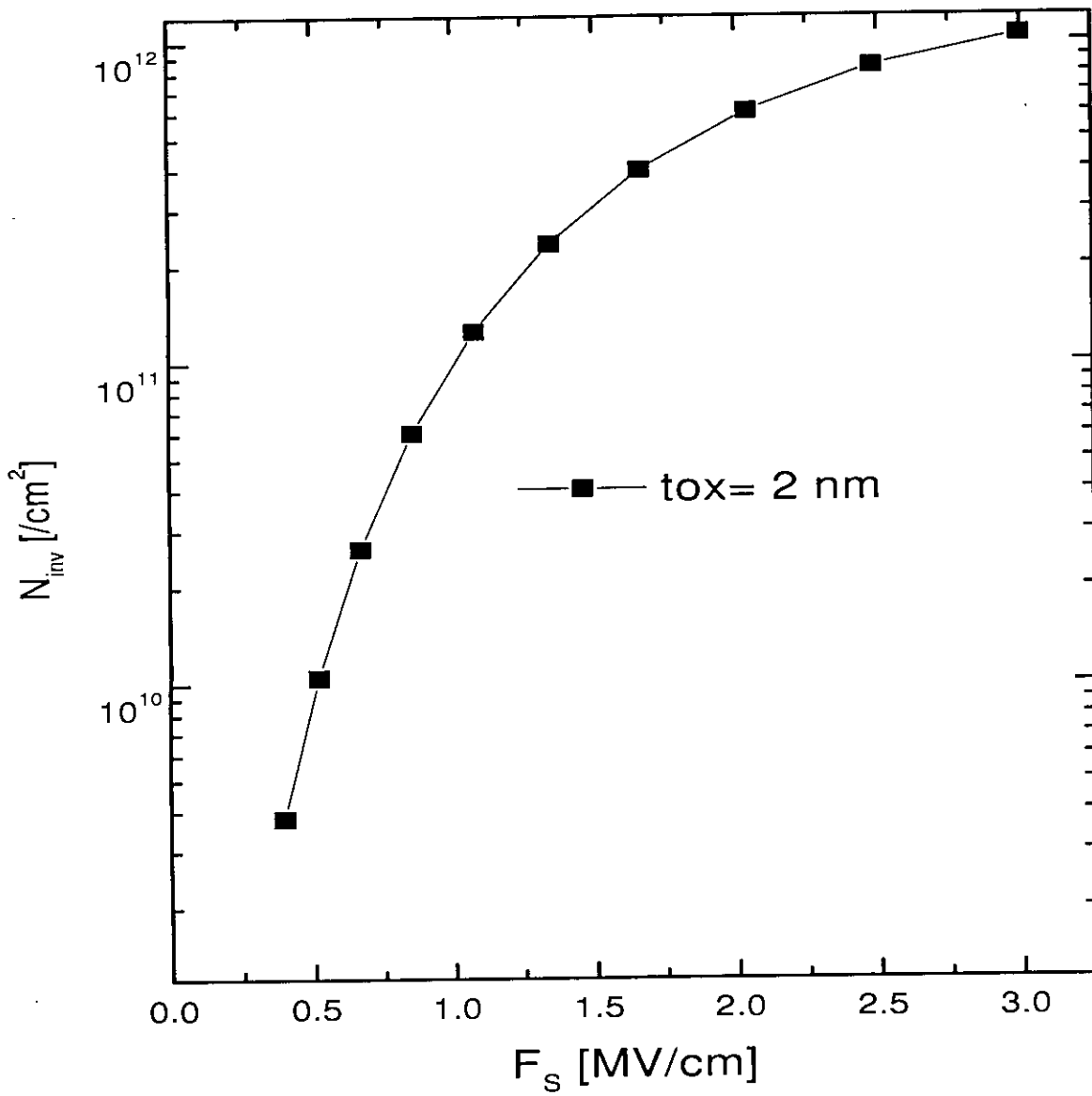


Fig. 4.3: Variation of carrier concentration with F_S for a given t_{ox} .

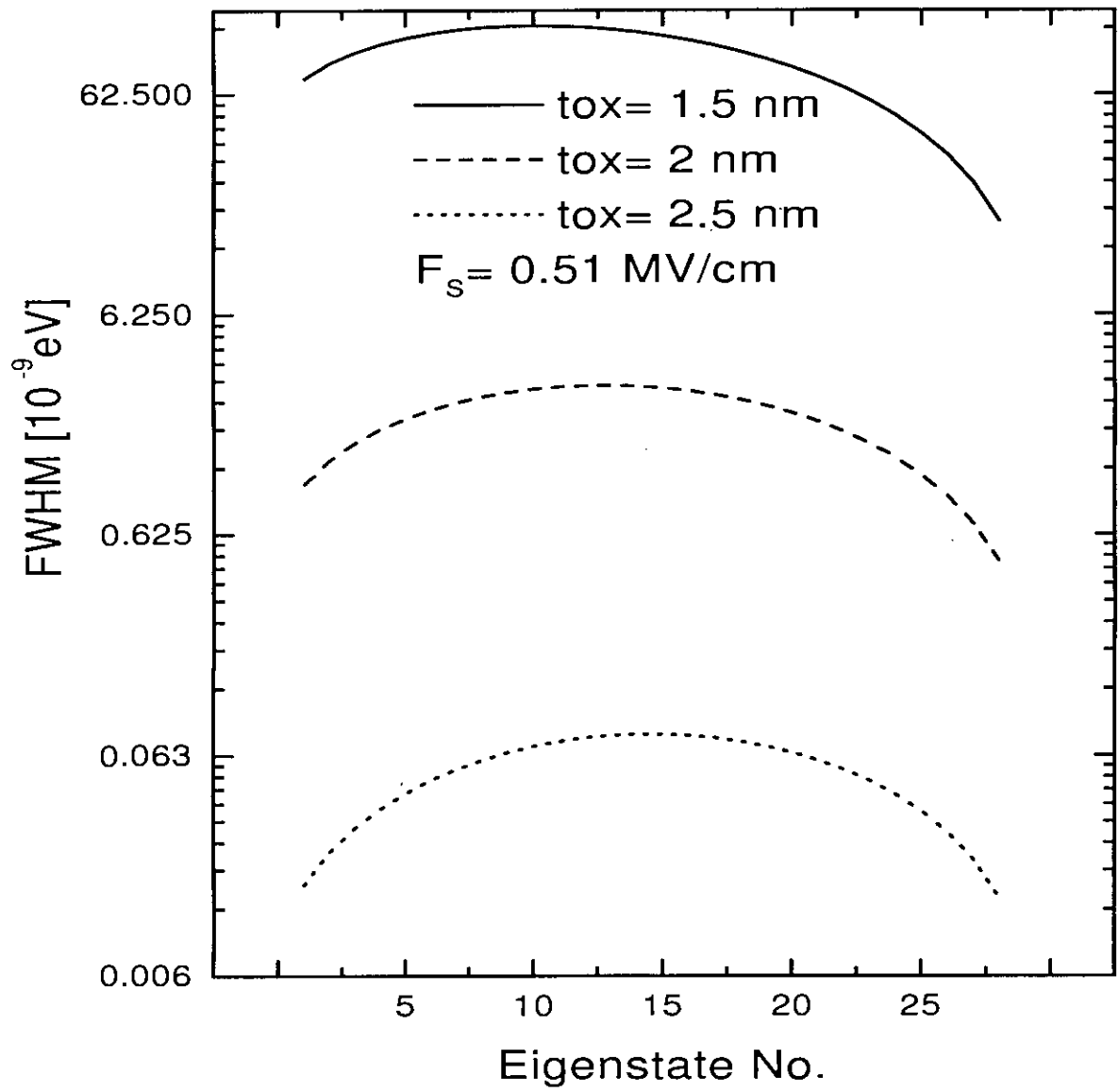


Fig. 4.4: Variation of FWHM with eigenstate number for different t_{ox} and a given F_s .

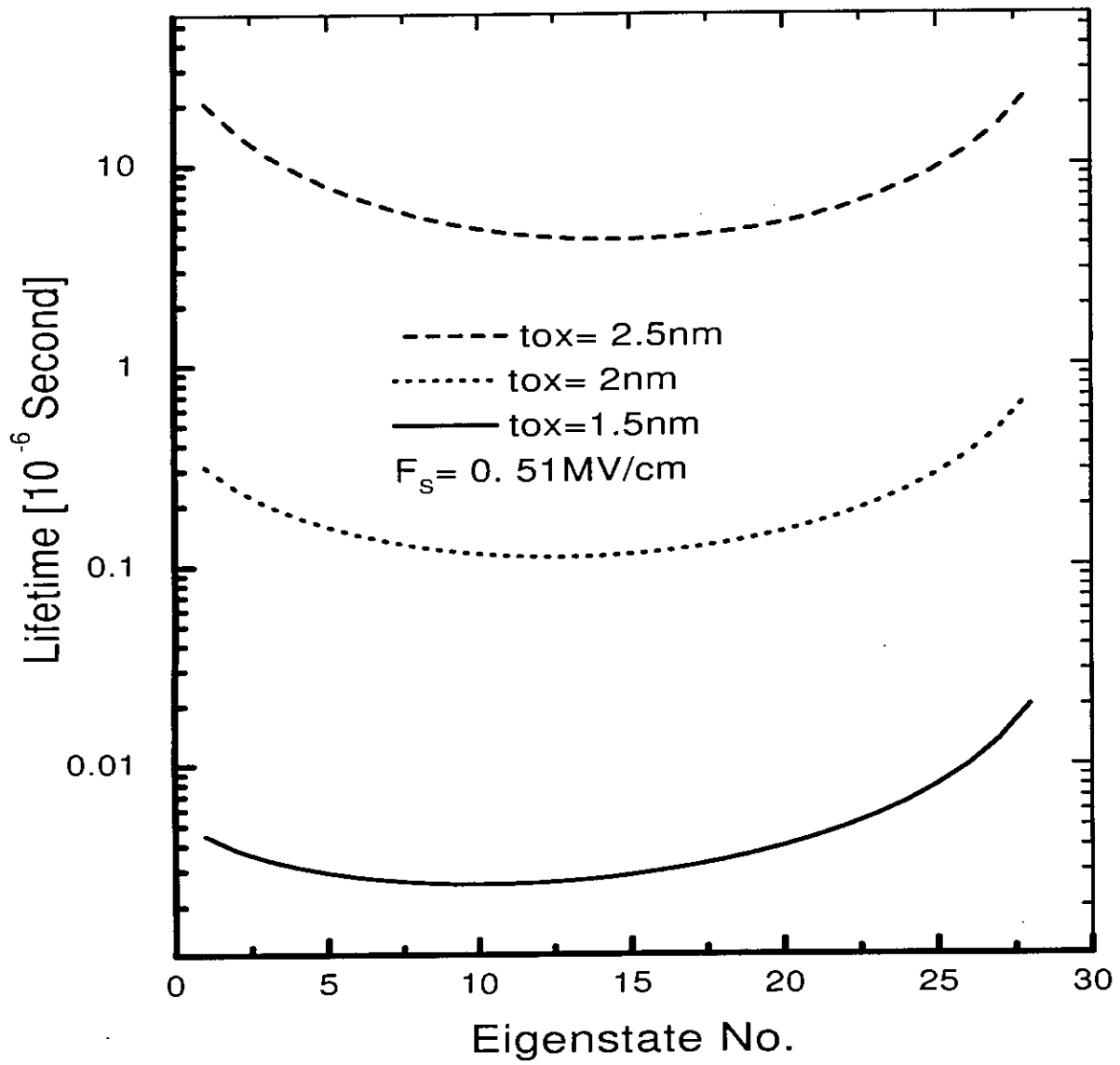


Fig. 4.5: Variation of lifetime with eigenstate number for different t_{ox} and a given F_s .

0

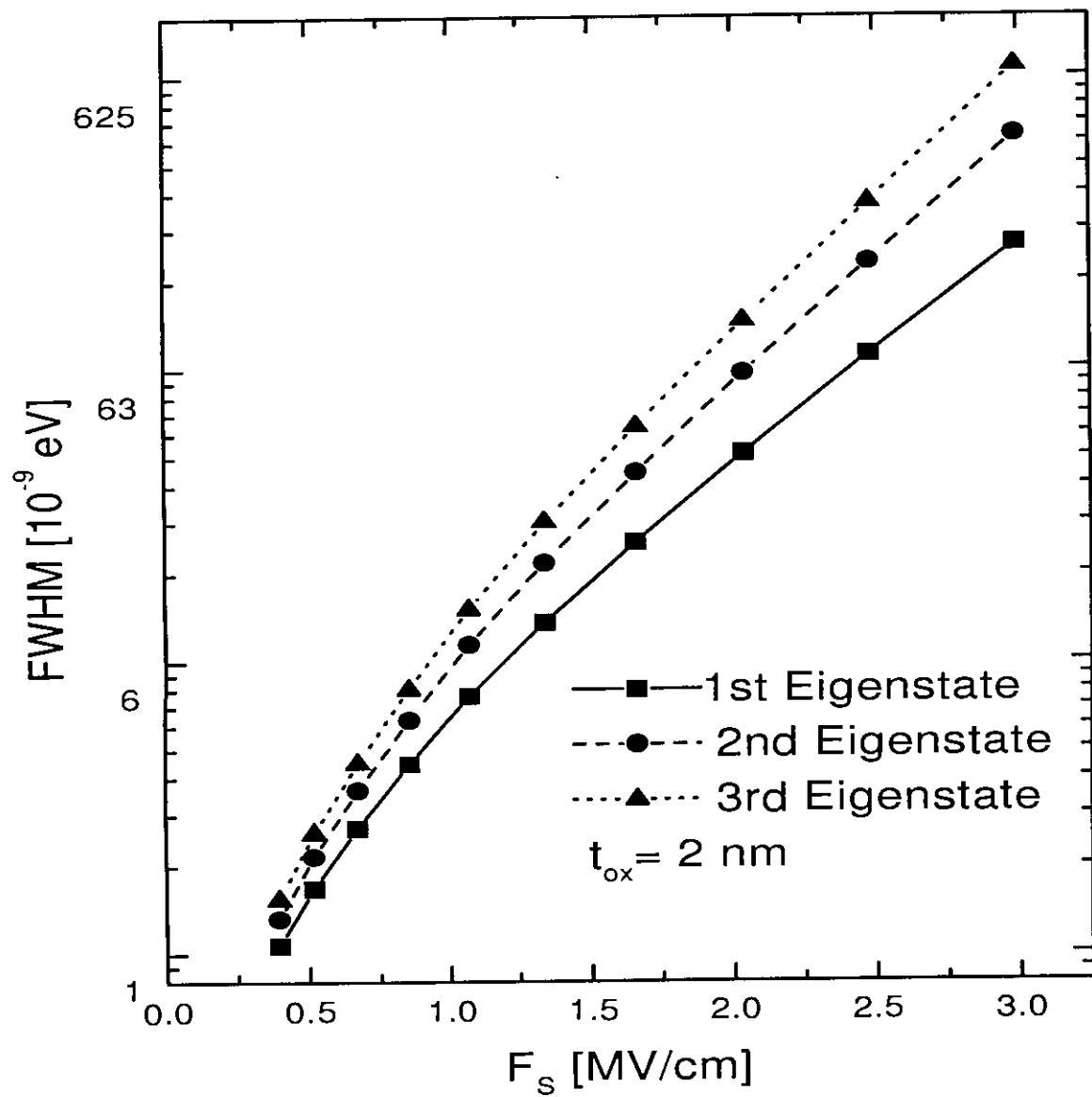


Fig. 4.6: Variation of FWHM for the first three eigenstates with F_S for a given t_{ox} .

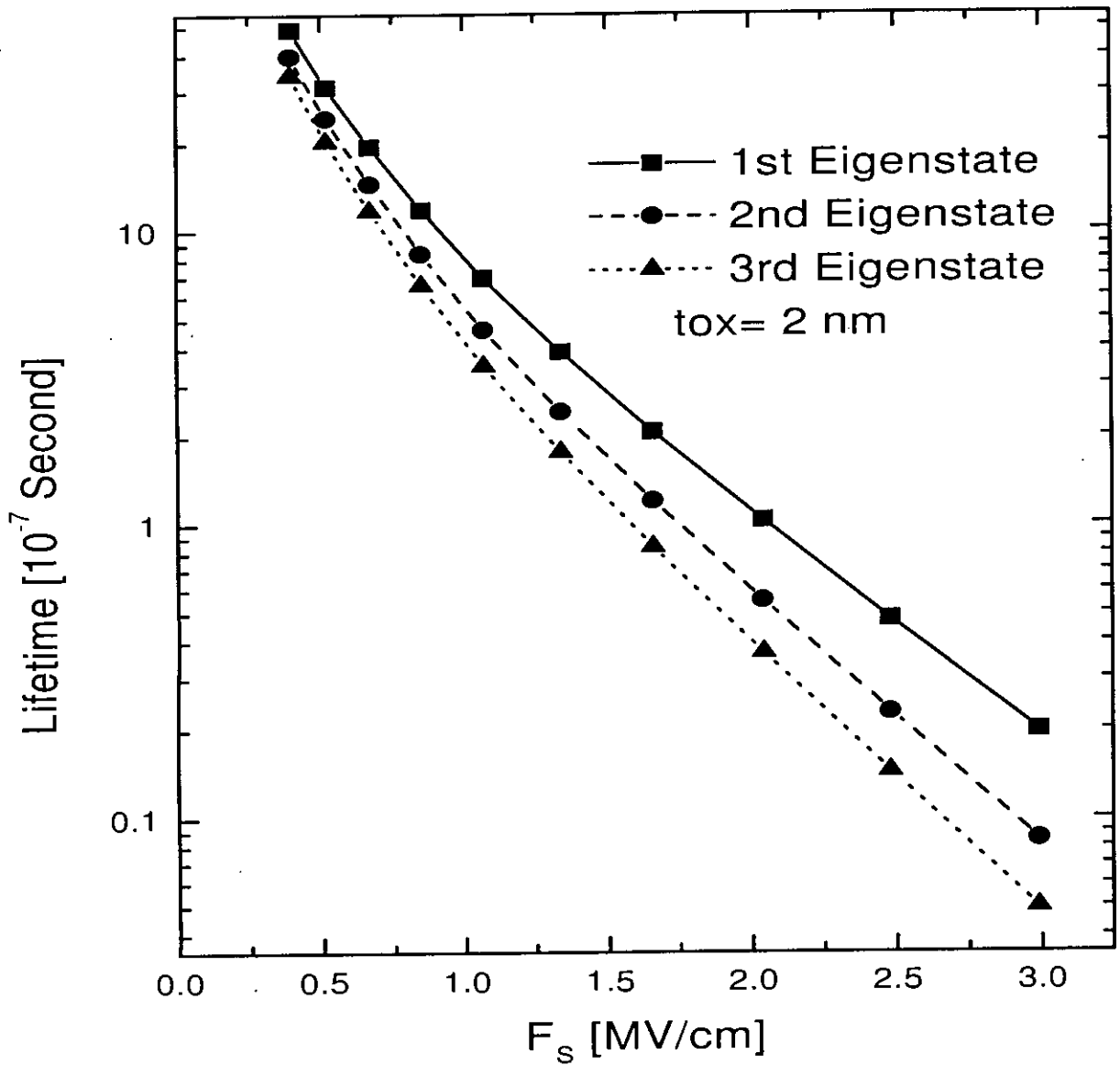


Fig. 4.7: Variation of lifetime of first three eigenstates with F_s for a given t_{ox} .

fields, the lifetime of the lowest state is higher than that of the third state by almost an order of magnitude. This is due to the fact that with increasing field, the barrier becomes increasingly narrower at higher energies (see Fig 4.2).

Figs. 4.8 and 4.9 are the plots of 1D DOS as function of energy around the first three eigenenergies evaluated at two different checkpoints $z = 28 \text{ \AA}$ and $z = 55 \text{ \AA}$ from the oxide-silicon interface, respectively. Although the magnitudes of the DOS are very different at these two points, their energy dependences are identical in the two figures. This signifies that the value of eigenenergy and the FWHM does not depend on the checkpoint as long as the point is within the potential well.

The variation of contributions of first three eigenstates to gate leakage current with F_S is shown in Fig 4.10. The contribution of the first and second eigenstate increases with the increase of F_S . However, the contribution of the third one starts decreasing at higher electric fields. It is due to the fact that, when the electric field increases, the value of the eigenenergy increases, and the differences between the Fermi energy and the third eigenenergy are greater at higher fields than that for lower one. This results in less concentration of electrons in that state at higher fields. Fig 4.10 also shows that the contribution to the direct tunneling current comes primarily from the lowest eigenstate.

Fig. 4.11 shows that the value of eigenenergies and the Fermi energy with the variation of surface field. It is seen from the figure that the differences between higher eigenenergies and Fermi energy increase for higher fields which results in less concentration of electrons in those eigenstates, as can be predicted from Eq. (2.5). So for higher fields, the current is contributed mainly by the lowest eigenstate.

The variation of total gate leakage current with F_S is shown in Fig. 4.12. It shows that, the gate current increases with the increase of surface electric field for a given t_{ox} . This increase of gate leakage current is due to the increase of both electron concentration in the inversion layer and the increase of FWHM with increasing F_S as seen in Figs. 4.3 and 4.6. Another feature of Fig 4.12 is that, for same F_S , with the increase of t_{ox} , the leakage current decreases. This is due to the fact that, with the increase of t_{ox} , the carrier concentration remains unchanged, but the lifetimes of electrons in any eigenstate increase, as can be seen from Fig. 4.5. So according to Eq. (4.1), with the increase of lifetime, the

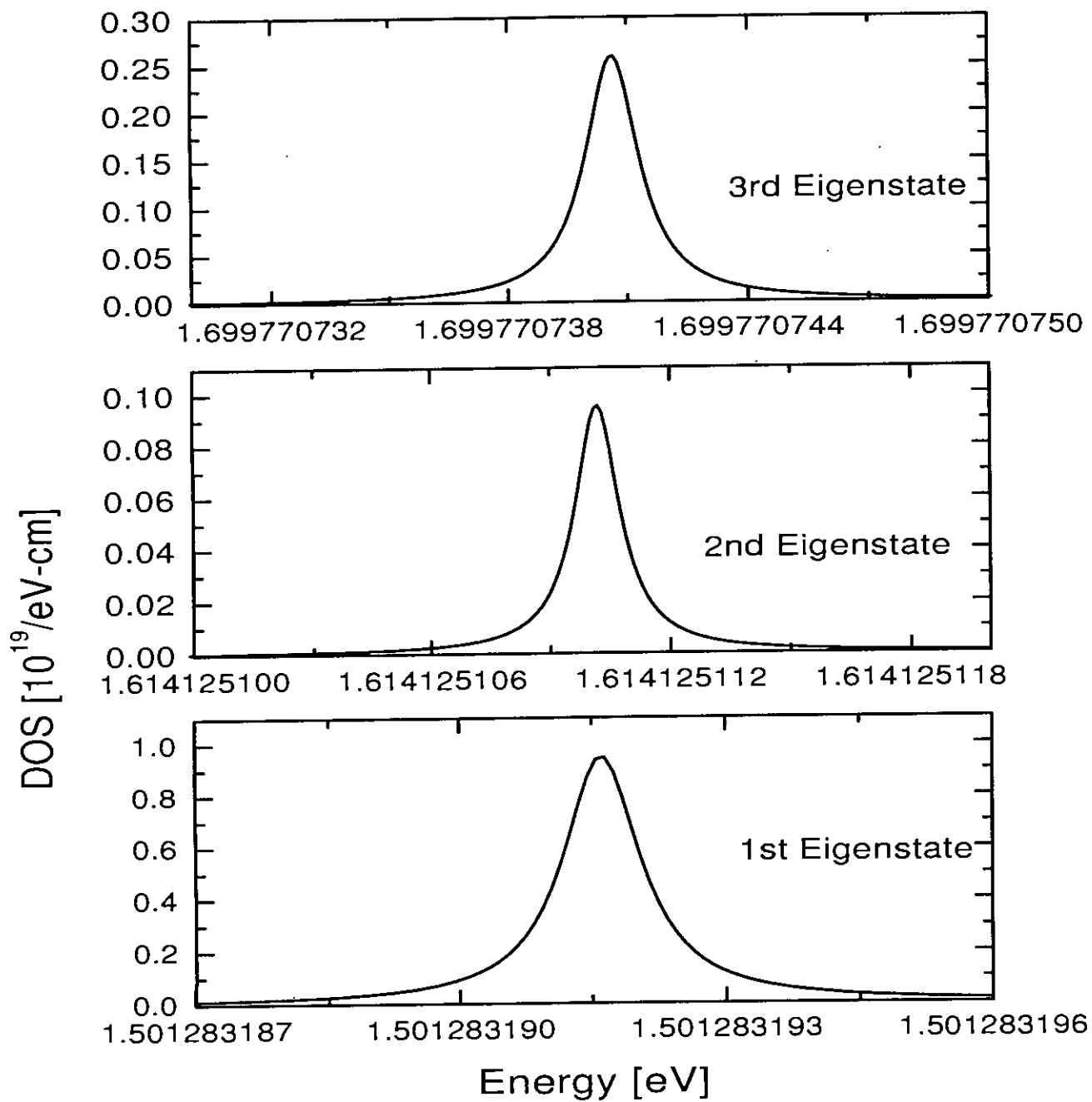


Fig. 4.8: Variation of DOS around the first three eigenenergies with energy for a given t_{ox} and F_S at checkpoint = 28 Å from the interface. $t_{ox} = 2$ nm, $F_S = 0.51$ MV/cm.

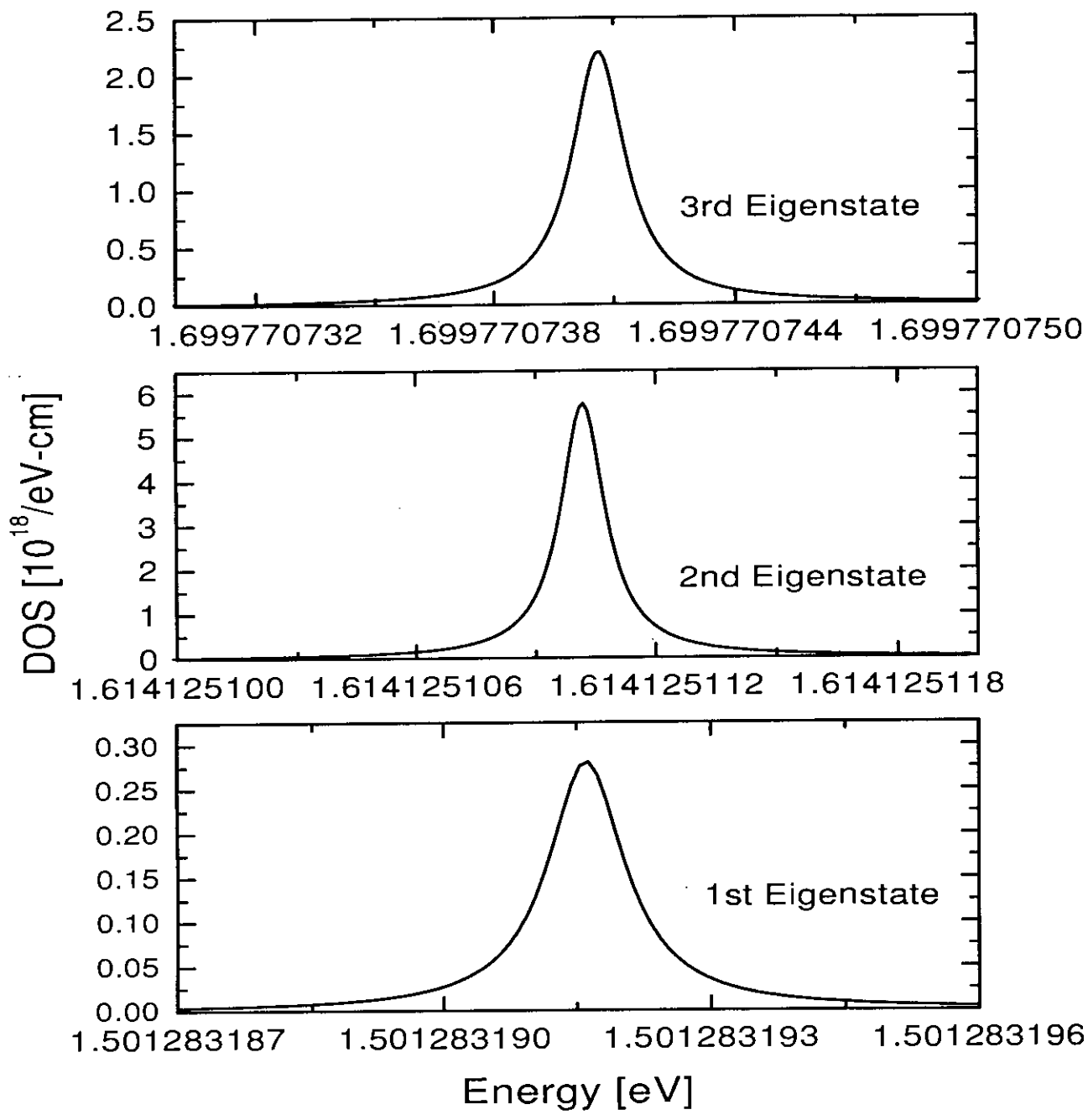


Fig. 4.9: Variation of DOS around the first three eigenenergies with energy for a given t_{ox} and F_S at checkpoint = 55 Å from the interface. $t_{ox} = 2$ nm, $F_S = 0.51$ MV/cm.

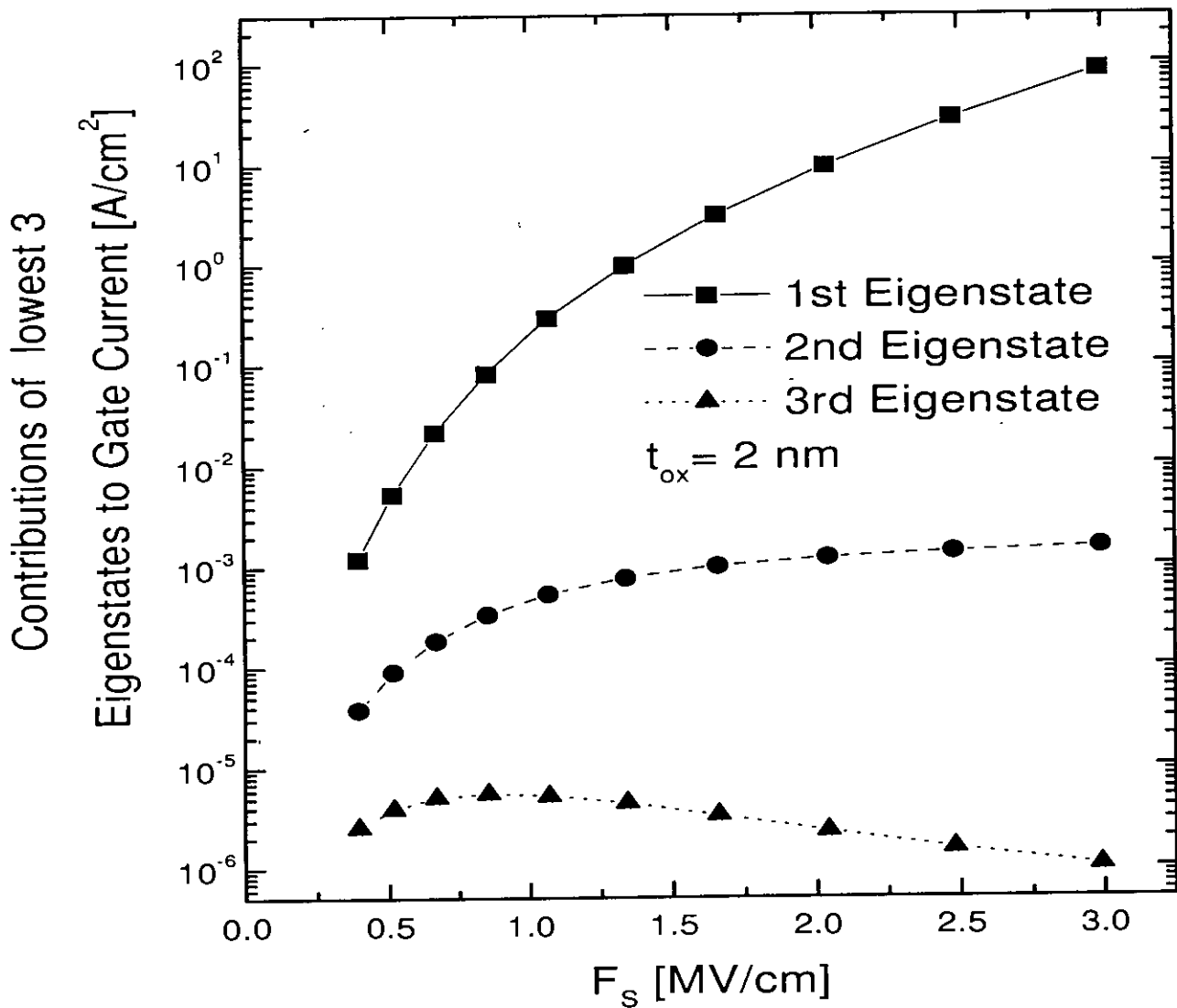


Fig. 4.10: Variation of contributions of first three eigenstates to gate leakage current with F_s for a given t_{ox} .

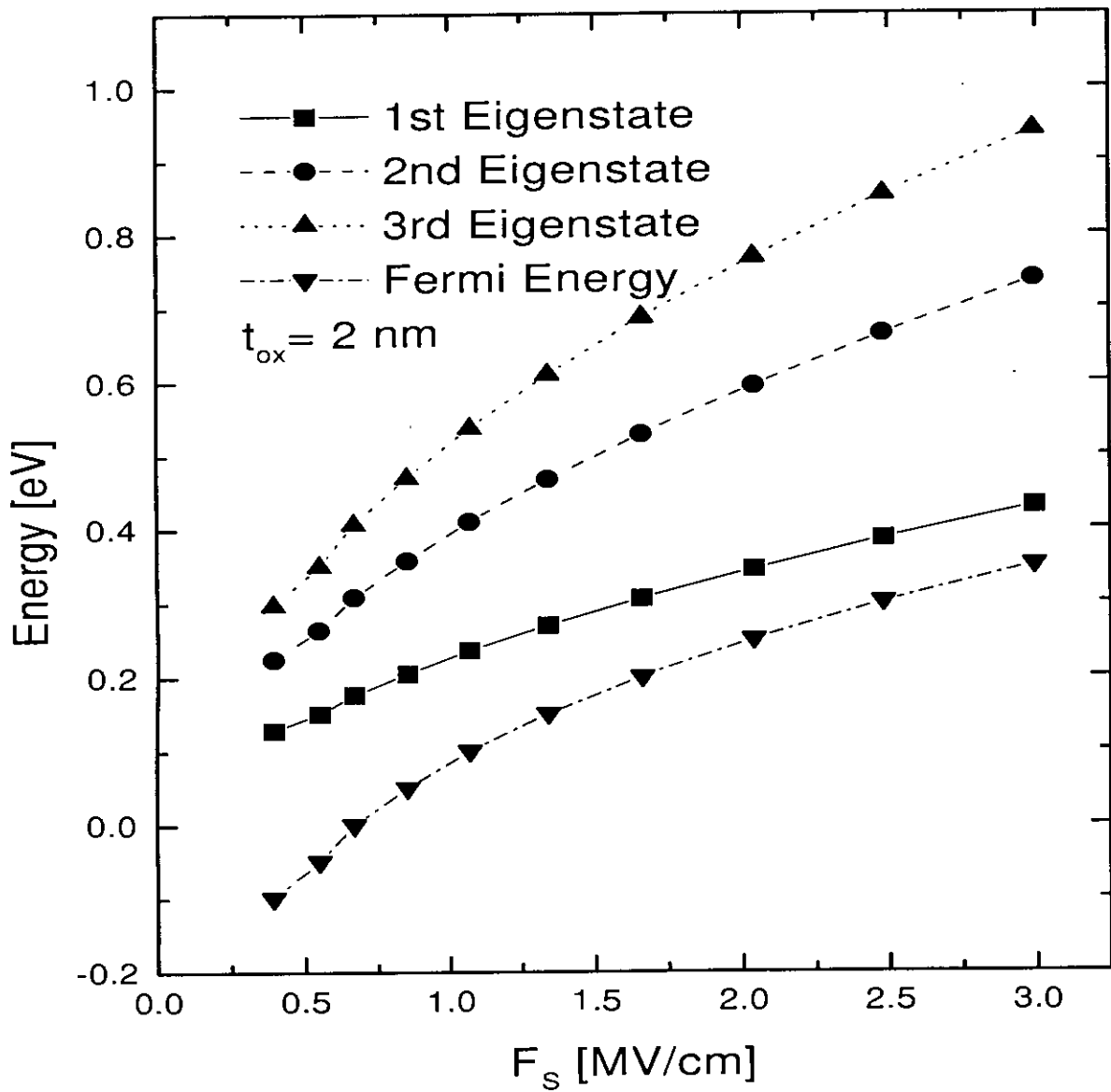


Fig. 4.11: Variation of 1st, 2nd, 3rd eigenenergy and Fermi energy with respect to bottom of the quantum well as functions of F_S for $t_{ox}=2 \text{ nm}$.

current will decrease.

Fig 4.13 shows the variation of same gate leakage current due to direct tunneling current with respect to gate voltage, where the gate voltage (V_g) is calculated using Eq. 4.3. In MOSFETs with thinner gate oxide, same surface electric field F_S leads to a lower gate voltage compared to those with thicker gate-oxide.

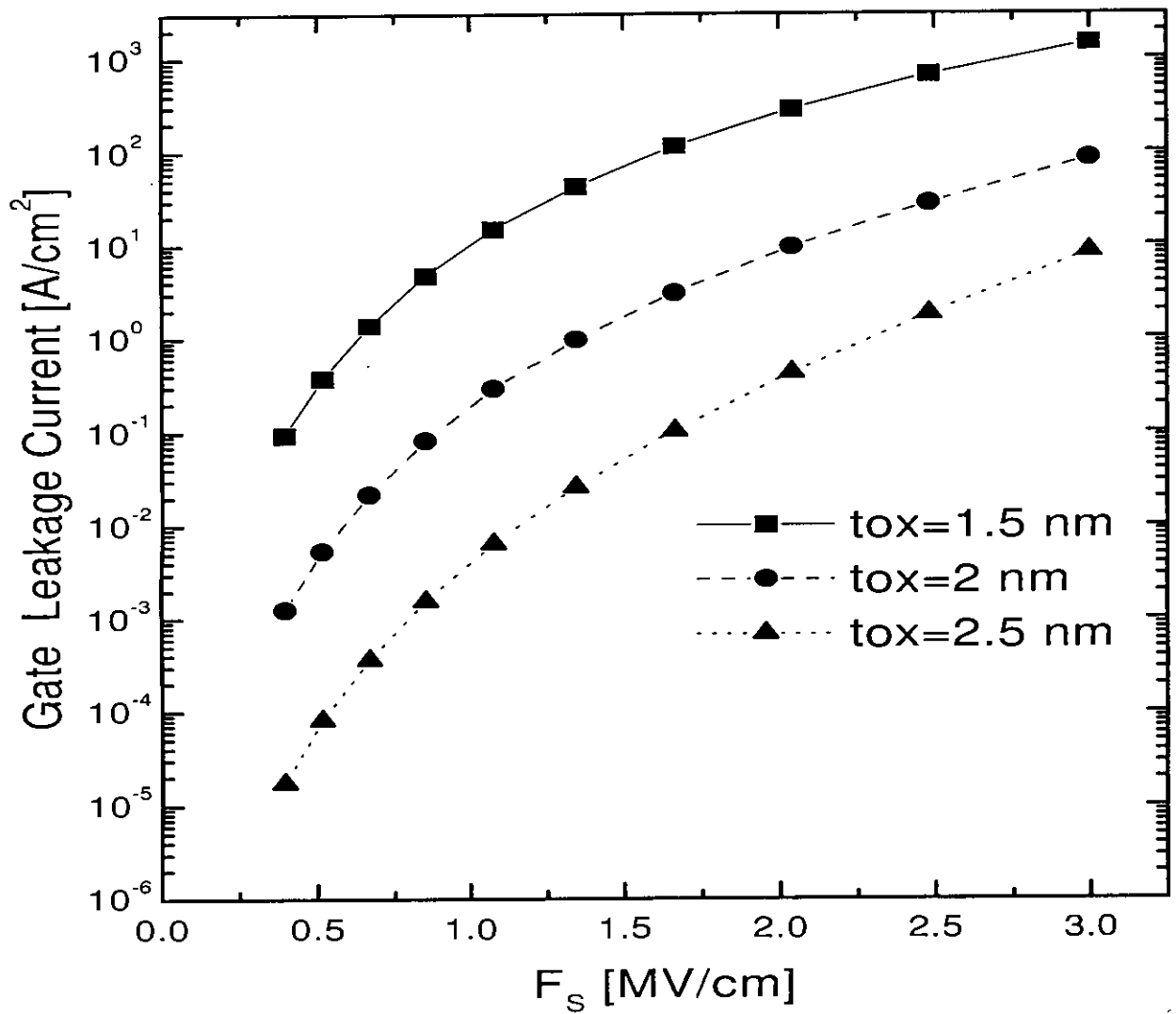


Fig. 4.12: Variation of gate leakage current with F_S for different t_{ox} .

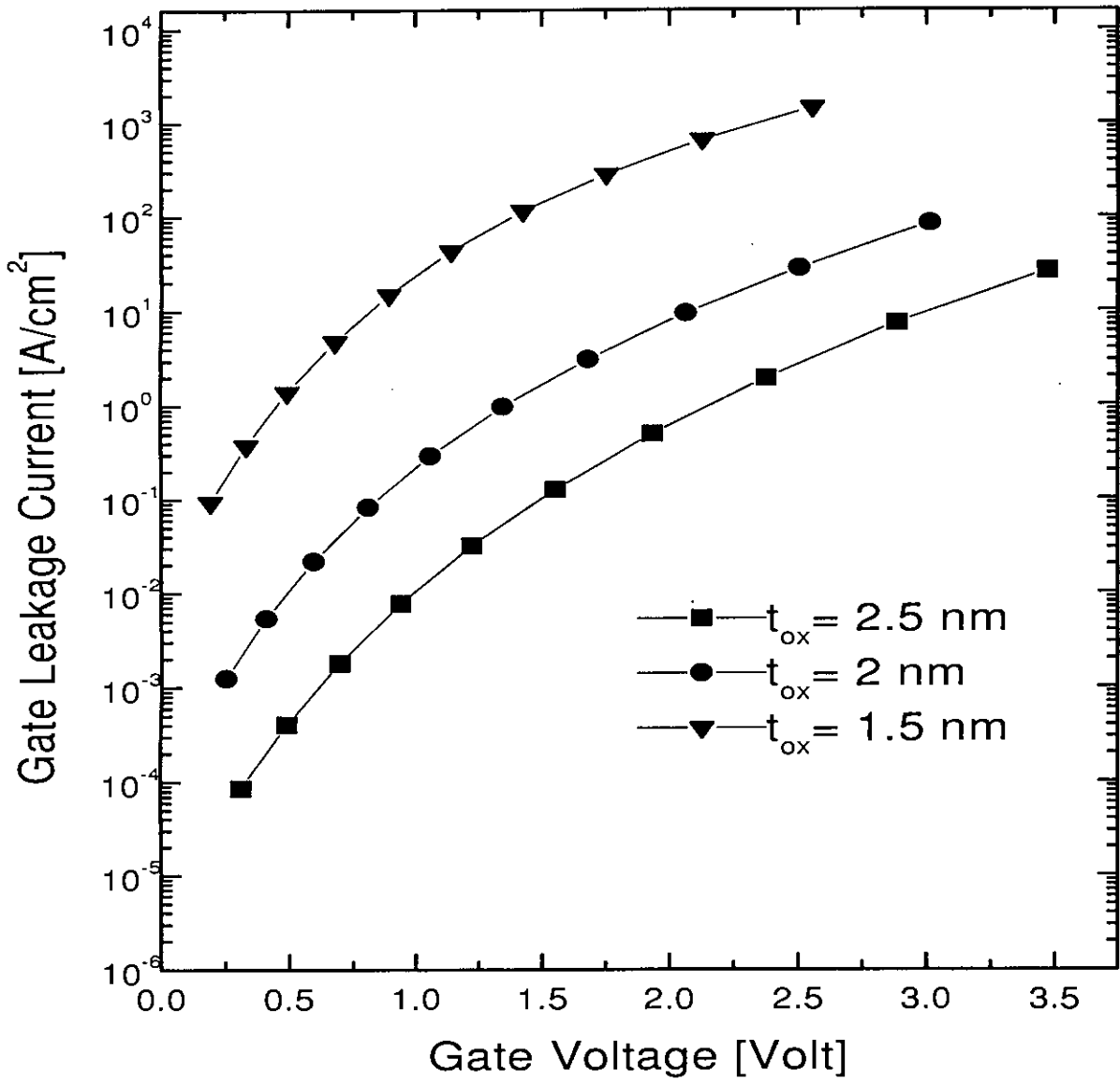


Fig. 4.13: Variation of gate leakage current with V_g for different t_{ox} .

Chapter 5

Direct Tunneling Current in the Presence of Scattering

It is known that due to the presence of phonons, defects, interface states and impurities, electrons tunneling through the oxide experience phase-breaking or inelastic scattering and hence, influence direct tunneling current. In this chapter, the effects of such scattering process on direct tunneling gate current are studied.

5.1 Theory

Inelastic scattering in oxide is represented by a position and energy dependent phase-breaking time $\tau_{coll}(z; E)$. The position and energy dependence of τ_{coll} is determined by the nature of the scattering processes present in the oxide. Inelastic scattering may be included in the Schrödinger's equation by an imaginary potential term jV_I , where $V_I = \hbar/2\tau_{coll}$. It is known that inelastic or phase-breaking scattering also causes broadening of the 1D DOS around the eigenenergies [32]. When broadening is due to more than one processes, the total broadening is expressed as the sum of the partial widths [35]. But, it has been shown elsewhere that for this relationship to hold true, all the broadening widths must be smaller than the separation between the eigenenergies [36]. Since this condition is satisfied by the populated states in Si inversion layers [33], it can be said that for the i th state,

$$\Gamma_{ti} = \Gamma_{li} + \Gamma_{si}, \quad (5.1)$$

where, Γ_t is the total broadening, Γ_s is the broadening due scattering only and Γ_l is the broadening due to coherent leakage only. It has been recently shown

that, although the states broaden in energy, the existing self-consistent formulation neglecting such broadening may be applied to determine the self-consistent potential profile, energies and wavefunctions [33].

Eq. (5.1) implies that the carriers in the inversion layer are lost by two mechanisms. First is due to direct tunneling of electrons from Si to gate electrode (represented by Γ_l) and the second is due to inelastic scattering of electrons (represented by Γ_s). The first process is already shown to contribute to gate leakage current. The second process also contributes to gate leakage current when the width of the oxide layer is thin. Total current is the sum of the two components.

The tunneling current associated with Γ_l can be calculated in a straight forward manner using Eq. (4.1), *i.e.*,

$$J_l = \sum_i \frac{eN_i}{\tau_{li}}, \quad (5.2)$$

where,

$$\tau_{li} = \frac{\hbar}{2\Gamma_{li}}. \quad (5.3)$$

Calculation of current associated with inelastic scattering is somewhat complicated. The quantity $\sum_i (eN_i/\tau_{si})$ (where $\tau_{si} = \hbar/2\Gamma_{si}$) represents the rate of loss of inversion charge due to inelastic scattering and hence the current due to inelastic scattering at the oxide-silicon interface. However, as the carriers experience inelastic collisions, a fraction of these will backscatter and return to the silicon inversion layer. In order to calculate this current considering multiple back-scattering effects, a formalism developed in [37] is used. According to this theory, the current flowing in the oxide at energy E_i is divided into a positive flowing and a negative flowing component. *i.e.*,

$$J_s(z; E_i) = J_s^+(z; E_i) + J_s^-(z; E_i). \quad (5.4)$$

Assuming that the current from any eigenenergy is not coupled to that of another eigenenergy via inelastic scattering, the left hand side of Eq. (5.4) becomes position independent from current conservation requirements. J_s^\pm are known to satisfy the following first order differential equations [37].

$$\frac{dJ_s^+(z, E_i)}{dz} = -\alpha^+(z, E_i)J_s^+(z, E_i) + r^+(z, E_i)[\alpha^+(z, E_i)J_s^+(z, E_i) + \alpha^-(z, E_i)J_s^-(z, E_i)], \quad (5.5)$$

$$\begin{aligned} \frac{dJ_s^-(z, E_i)}{dz} &= -\alpha^-(z, E_i)J_s^-(z, E_i) + r^-(z, E_i)[\alpha^+(z, E_i)J_s^+(z, E_i) \\ &+ \alpha^-(z, E_i)J_s^-(z, E_i)], \end{aligned} \quad (5.6)$$

here, $r^\pm(z, E_i) = [|v_g^\pm(z, E_i)|] / [|v_g^+(z, E_i)| + |v_g^-(z, E_i)|]$ represents the probability that an electron scattered at z will travel in $\pm z$ direction, v_g^\pm is group velocity of an electron moving in $\pm z$ direction. $\alpha^\pm(z, E_i) = 1 / (\tau_{coll}(z)v_g^\pm(z, E_i))$ is the linear scattering rate. Eqs.(5.5) and (5.6) can be solved analytically for oxide region if the injected currents at the two boundaries $J_{inj}^+(z = -t_{ox}, E_i)$ and $J_{inj}^-(z = 0, E_i)$ are known. Here silicon-oxide interface is treated to be $z = 0$. Since electrons are injected into the oxide only from the right (from the semiconductor) and there is no injection of electrons from the left (from the gate electrode), the boundary conditions used are, $J_{inj}^+(z = -t_{ox}, E_i) = 0$ and $J_{inj}^-(z = 0, E_i) = -eN_i/\tau_{si}$. Solutions of Eqs.(5.5) and (5.6), when substituted in Eq. (5.4) gives [37]

$$J_s(E_i) = \frac{-eN_i/\tau_{si}}{1 + B(-t_{ox}, 0, E_i)}, \quad (5.7)$$

where,

$$B(-t_{ox}, 0, E_i) = \int_{-t_{ox}}^0 \xi(z', E_i)A(z', 0, E_i)dz', \quad (5.8)$$

$$\xi(z, E_i) = \frac{1}{\tau_{coll}(z, E_i)} \left[\frac{v_g^+(z, E_i)}{[v_g^+(z, E_i) - v_g^-(z, E_i)] v_g^-(z, E_i)} \right], \quad (5.9)$$

$$A(a, 0, E_i) = e^{-\int_a^0 \beta(z, E_i)dz}, \quad (5.10)$$

and,

$$\beta(z, E_i) = \frac{1}{\tau_{coll}(z, E_i)} \left[\frac{1}{v_g^+(z, E_i)} + \frac{1}{v_g^-(z, E_i)} \right]. \quad (5.11)$$

Considering the magnitudes of the current in Eq. (5.7) for all the eigenstates,

$$J_s = \sum_i |J_s(E_i)|, \quad (5.12)$$

and the total gate leakage current due to direct tunneling in the presence of inelastic scattering in the oxide is,

$$J = J_l + J_s. \quad (5.13)$$

5.2 Results and Discussions

In this section, results of numerical calculations are presented. In these calculations, energy dependence of τ_{coll} is neglected and two different position dependences are considered. First, the validity of Eq. (5.1) is studied. Γ_l is obtained from a structure with finite t_{ox} that has no phase-breaking processes. Γ_s is obtained from a device having phase-breaking processes with t_{ox} approaching infinity, since, there is no direct tunneling when the oxide width is very large. The broadening in a structure containing finite t_{ox} and phase-breaking scattering in oxide gives Γ_t . In all three cases, identical inversion potential profile is considered. Two profiles of τ_{coll} have been used, these are, constant value throughout the oxide and an exponential function, that decays from the silicon-oxide interface towards gate-electrode. The exponential form is described for $-t_{ox} < z < 0$ by the equation,

$$\tau_{coll} = \tau_o e^{z/l}. \quad (5.14)$$

The characteristic length, l has been taken to be 10 nm. This is consistent with the trap distribution of profile as reported in [38]. Tables 5.1- 5.4 show that indeed, Eq. (5.1) holds true. Moreover, it is observed that the effects of scattering are more pronounced at lower electric fields and as expected, at smaller values of τ_{coll} . It is also observed that although Γ_l exhibits non-monotonic behaviour, Γ_s decreases monotonically with increasing eigennumbers.

The current due to scattering is given by the Eq. (5.7), where B is given by Eq. (5.8). B is a dimensionless quantity, that represents the effects of backscattering on J_s . The variation of B for lowest two eigenstates with F_S is shown in Fig. 5.1 for constant collision time. It is seen that B is very sensitive to the changes in either the surface electric field or the oxide thickness. Increase in F_S or decrease in t_{ox} causes exponential decrease in the value of B. Fig. 5.2 shows the variation of B for lowest eigenstate for different values and profiles of collision time. The figure signifies that the chosen collision time profile variations has little impact on the value of B.

Fig. 5.3 shows the variation of lifetimes with No of eigenstate, for $t_{ox} = 2$ nm and $F_S = 0.51$ MV/cm, without scattering and with scattering, for two collision times (constant). The effects of collision time on electron lifetime is seen here. The same phenomenon for $F_S = 1.66$ MV/cm is shown in Fig 5.4. Figs. 5.3 and 5.4

Eigen-number	Γ_t (neV)	Γ_l (neV)	Γ_s (neV)	$\Gamma_t + \Gamma_s$ (neV)	% Error (10^{-4})
1	2.162528	1.052517	1.110012	2.16253	-0.83
2	2.376464	1.351437	1.025024	2.376461	1.64
3	2.574864	1.619789	0.9550689	2.574858	2.45
4	2.760032	1.866953	0.8930779	2.760031	0.33
5	2.929936	2.093552	0.8363741	2.929926	3.28
6	3.08168	2.298096	0.7835866	3.081683	-0.78
7	3.212368	2.478448	0.7339049	3.212353	4.68
8	3.319376	2.63256	0.6868002	3.31936	4.71
9	3.400512	2.758608	0.6419057	3.400514	-0.35
10	3.454096	2.855136	0.5989576	3.454094	0.69
11	3.478928	2.921168	0.5577575	3.478925	0.86
12	3.474416	2.956272	0.5181521	3.474424	-2.42
13	3.440464	2.960432	0.4800176	3.44045	4.02
14	3.377456	2.934192	0.4432626	3.377455	0.44
15	3.28632	2.878512	0.407803	3.286315	1.55
16	3.1684	2.794832	0.3735721	3.168404	-1.33
17	3.025424	2.684912	0.3405205	3.025432	-2.58
18	2.859456	2.550864	0.3085936	2.859458	-0.53
19	2.672816	2.395056	0.2777571	2.672814	0.89
20	2.46808	2.220112	0.2479713	2.468083	-1.46
21	2.247952	2.028736	0.2192086	2.247944	3.48
22	2.015216	1.82376	0.1914365	2.015197	9.55
23	1.77272	1.60808	0.1646339	1.772714	3.39
24	1.52328	1.384496	0.1387746	1.523271	5.91
25	1.26968	1.155856	0.1138384	1.269695	-11.36
26	1.014608	0.9248158	0.089807	1.014623	-14.51
27	0.7605602	0.6939043	0.06665918	0.7605635	-4.35
28	0.5099041	0.4655202	0.04437934	0.5098996	8.84

Table 5.1: Relationship among calculated Γ_t , Γ_l and Γ_s for different eigenstates for $F_S = 0.51$ MV/cm, $\tau_{coll} = 10^{-9}$ s and $t_{ox} = 2$ nm.

Eigen-number	Γ_t (neV)	Γ_l (neV)	Γ_s (neV)	$\Gamma_t + \Gamma_s$ (neV)	% Error (10^{-4})
1	12.1527	1.05252	11.1001	12.1526	2.23
2	11.6017	1.35144	10.2502	11.6017	1.76
3	11.1705	1.61979	9.55067	11.1705	1.67
4	10.7977	1.86695	8.93077	10.7977	2.17
5	10.4573	2.09355	8.36373	10.4573	1.52
6	10.134	2.2981	7.83587	10.134	-0.06
7	9.8175	2.47845	7.33906	9.8175	-0.03
8	9.50058	2.63256	6.868	9.50056	1.74
9	9.17766	2.75861	6.41907	9.17768	-1.70
10	8.84472	2.85514	5.98958	8.84472	-0.034
11	8.49877	2.92117	5.57758	8.49875	1.95
12	8.13779	2.95627	5.18152	8.13779	0
13	7.76062	2.96043	4.80018	7.76061	2.05
14	7.3668	2.93419	4.43262	7.36682	-2.12
15	6.95653	2.87851	4.07803	6.95654	-2.38
16	6.53056	2.79483	3.73573	6.53056	-0.05
17	6.0901	2.68491	3.4052	6.09011	-2.42
18	5.63682	2.55086	3.08594	5.6368	2.72
19	5.17262	2.39506	2.77758	5.17264	-3.08
20	4.69982	2.22011	2.47973	4.69984	-3.52
21	4.22082	2.02874	2.19208	4.22082	0.07
22	3.73813	1.82376	1.91438	3.73814	-4.18
23	3.25442	1.60808	1.64632	3.2544	4.62
24	2.77224	1.3845	1.38774	2.77224	0.22
25	2.29422	1.15586	1.13838	2.29424	-6.81
26	1.82286	0.924816	0.898063	1.82288	-8.57
27	1.3605	0.693904	0.666592	1.3605	-0.22
28	0.909328	0.46552	0.443792	0.909312	17.19

Table 5.2: Relationship among calculated Γ_t , Γ_l and Γ_s for different eigenstates for $F_S = 0.51$ MV/cm, $\tau_{coll} = 10^{-10}$ s and $t_{ox} = 2$ nm.

Eigen-number	Γ_t (10^{-7} eV)	Γ_l (10^{-7} eV)	Γ_s (neV)	$\Gamma_l + \Gamma_s$ (10^{-7} eV)	% Error (10^{-4})
1	1.71916	1.65709	6.20675	1.71916	-0.17
2	3.95003	3.89848	5.15558	3.95004	-0.97
3	6.71581	6.67336	4.24631	6.71582	-2.24
4	9.28666	9.25254	3.4137	9.28668	-2.68
5	10.7704	10.744	2.63865	10.7704	-1.72
6	10.505	10.4859	1.91788	10.505	-2.56
7	8.374	8.36149	1.25206	8.37401	-1.03
8	4.85915	4.85269	0.646083	4.85915	0.65

Table 5.3: Relationship among calculated Γ_t , Γ_l and Γ_s for different eigenstates for $F_S = 3$ MV/cm, $\tau_{coll} = 10^{-9}$ s and $t_{ox} = 2$ nm.

Eigen-number	Γ_t (10^{-7} eV)	Γ_l (10^{-7} eV)	Γ_s (10^{-7} eV)	$\Gamma_l + \Gamma_s$ (10^{-7} eV)	% Error (10^{-2})
1	2.27774	1.65709	0.620675	2.27777	-0.11
2	4.41397	3.89848	0.51556	4.41404	-0.16
3	7.09782	6.67336	0.42463	7.09799	-0.23
4	9.59368	9.25254	0.341371	9.59392	-0.24
5	11.0076	10.744	0.263864	11.0079	-0.23
6	10.6773	10.4859	0.191787	10.6776	-0.28
7	8.48648	8.36149	0.125205	8.48669	-0.25
8	4.91718	4.85269	0.0646096	4.9173	-0.23

Table 5.4: Relationship among calculated Γ_t , Γ_l and Γ_s for different eigenstates for $F_S = 3$ MV/cm, $\tau_{coll} = 10^{-10}$ s and $t_{ox} = 2$ nm.

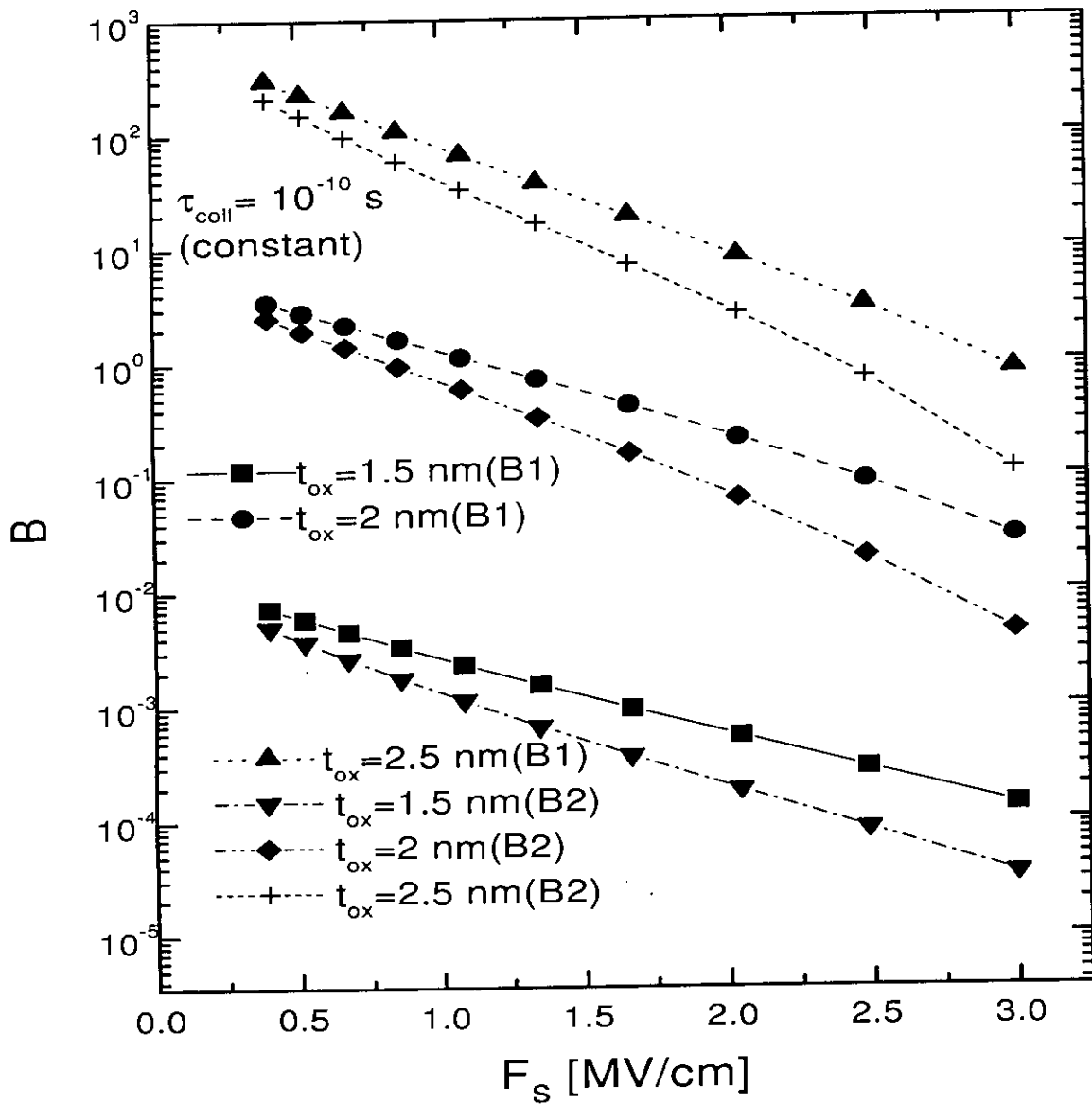


Fig. 5.1: Variation of B for lowest two eigenenergies for different t_{ox} . B1 corresponds to the lowest state and B2 corresponds to the second lowest state.

F_s (MV/cm)	$I_G(A/cm^2)$ Exponential profile ($\tau_o = 10^{-10}s$)	$I_G(A/cm^2)$ Constant profile ($\tau_{coll} = 10^{-10}s$)
0.395	51.30125	51.61685
0.517	216.4169	216.4129
0.669	843.5441	837.6783
0.853	3025.785	2982.124
1.07	9947.525	9728.363
1.34	29854.06	28987.26
1.66	81668.08	78872.58
2.04	205335.9	197958.4
2.48	489438.9	473572.6
3.00	1176310	1148238

Table 5.5: Comparison of the value of gate leakage current for exponential and constant profiles of τ_{coll} . $t_{ox} = 2$ nm.

show an interesting effect of phase-breaking scattering on the lifetimes of the quasi-bound states. In the absence of any scattering the lifetimes of populated states (lower eigenenergies) decrease with increasing energy. However, as the phase-breaking scattering becomes stronger, this trend becomes weaker and at sufficient strong scattering, lifetimes of these states even increase with increasing energy. However, the trend of lifetimes of higher energy states remain unaffected by phase-breaking scattering. This observation can be explained in terms of results presented in Tables 5.1- 5.4.

The effect of using different scattering profile has little impact on the value of simulated gate leakage current. This fact is illustrated in Table. 5.5. So, although the exponential variation of scattering potential is more realistic, for ease of numerical implementation, the constant profile may be used without introducing significant error.

Figs. 5.6 and 5.5 are the plots of direct tunneling current in the presence of phase-breaking scattering as a function of gate voltage for two different values of τ_{coll} . These results have also been compared to the case when there is no scattering. It is observed that scattering increases the gate current and has more pronounced effects in devices with thicker gate oxides. The current in the device with $t_{ox}=1.5$ nm is almost unaffected by scattering. It is also found that scattering effects are more significant at lower gate voltages. These results explain

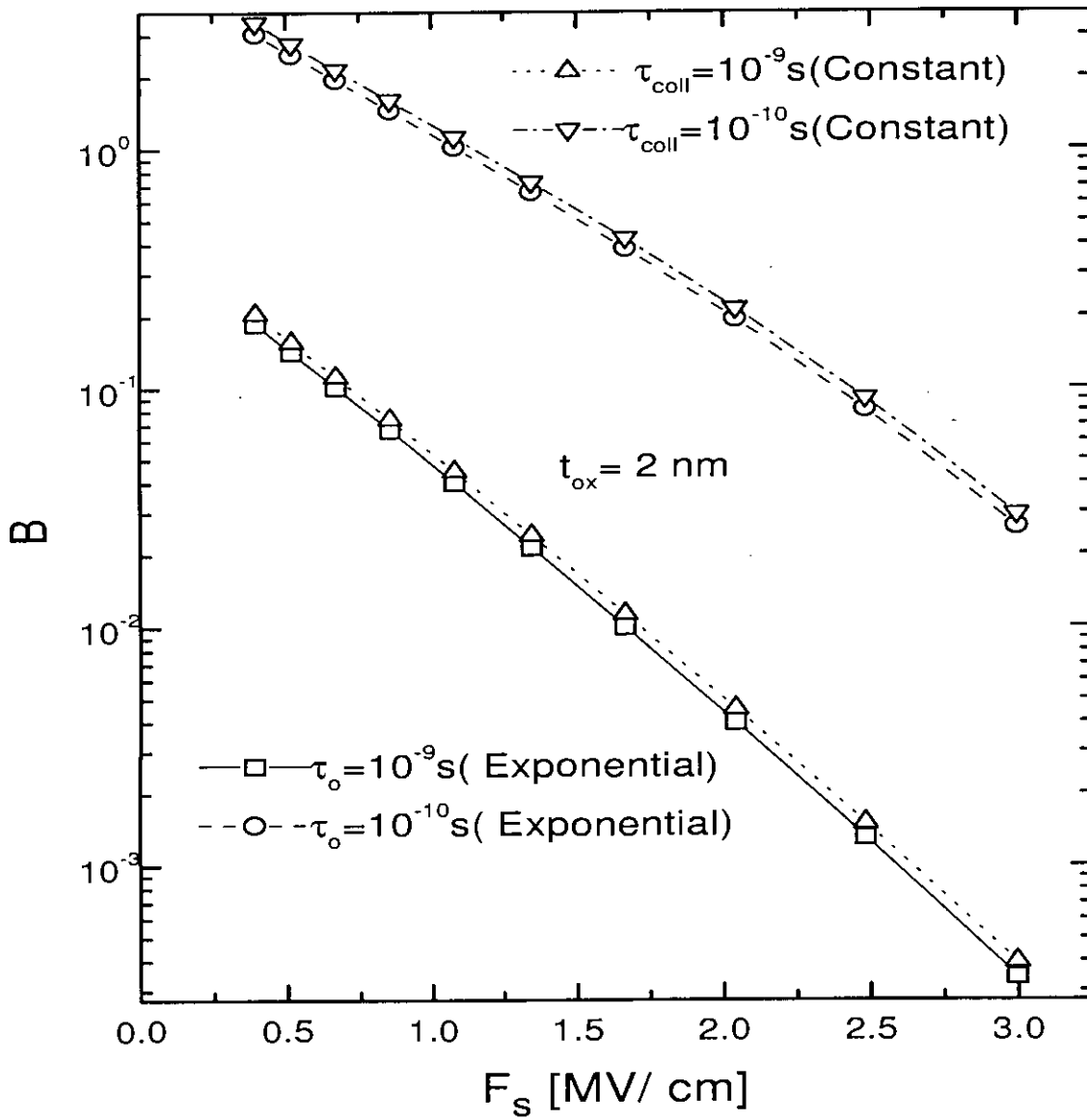


Fig. 5.2: Variation of B for 1st eigenenergy for two different values of collision time and two different collision time profiles.

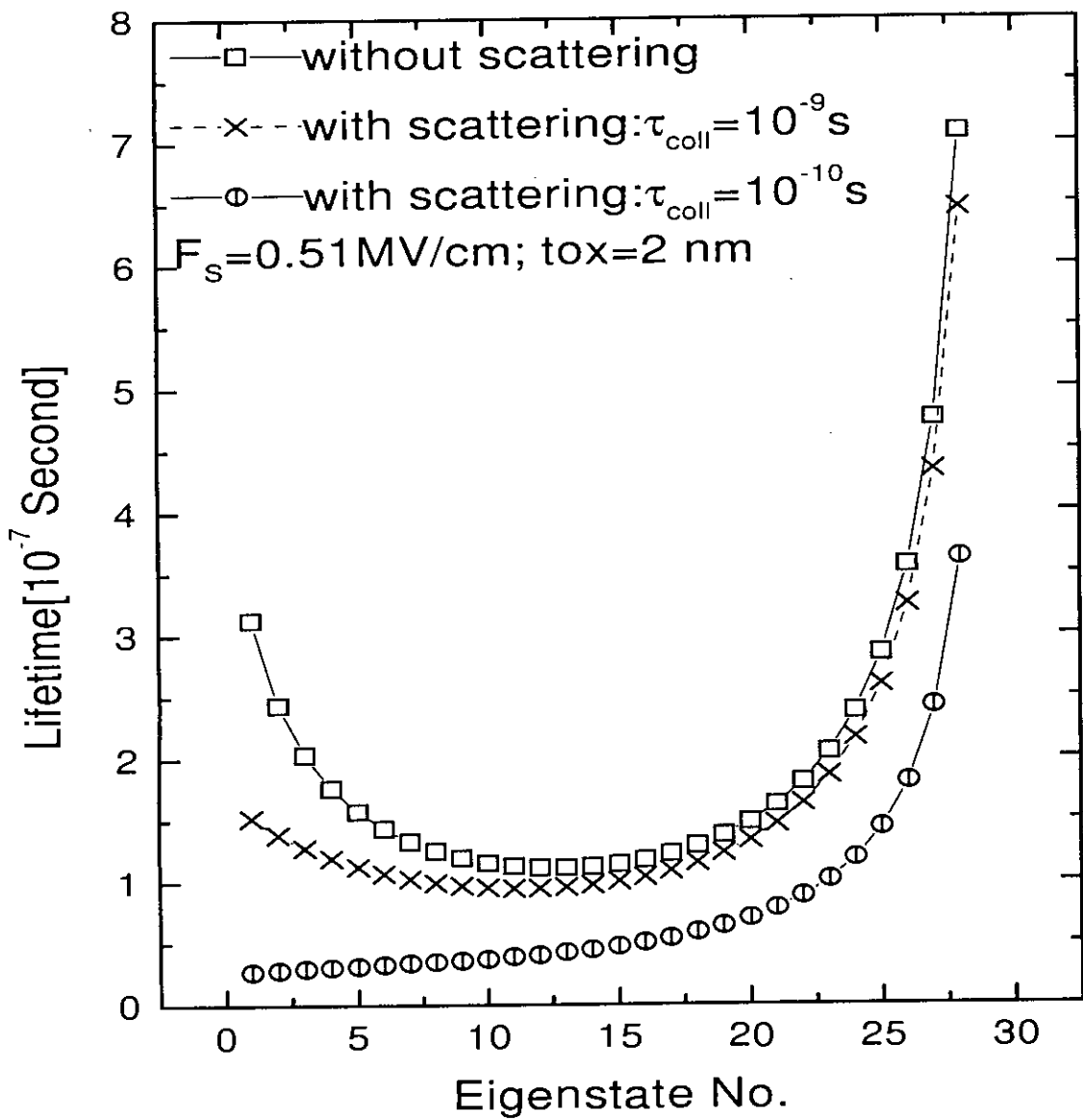


Fig. 5.3: Variation of lifetimes of different eigenstates for two different values of collision time and two different collision time profile with $F_s = 0.51 \text{ MV/cm}$ and $t_{ox} = 2 \text{ nm}$.

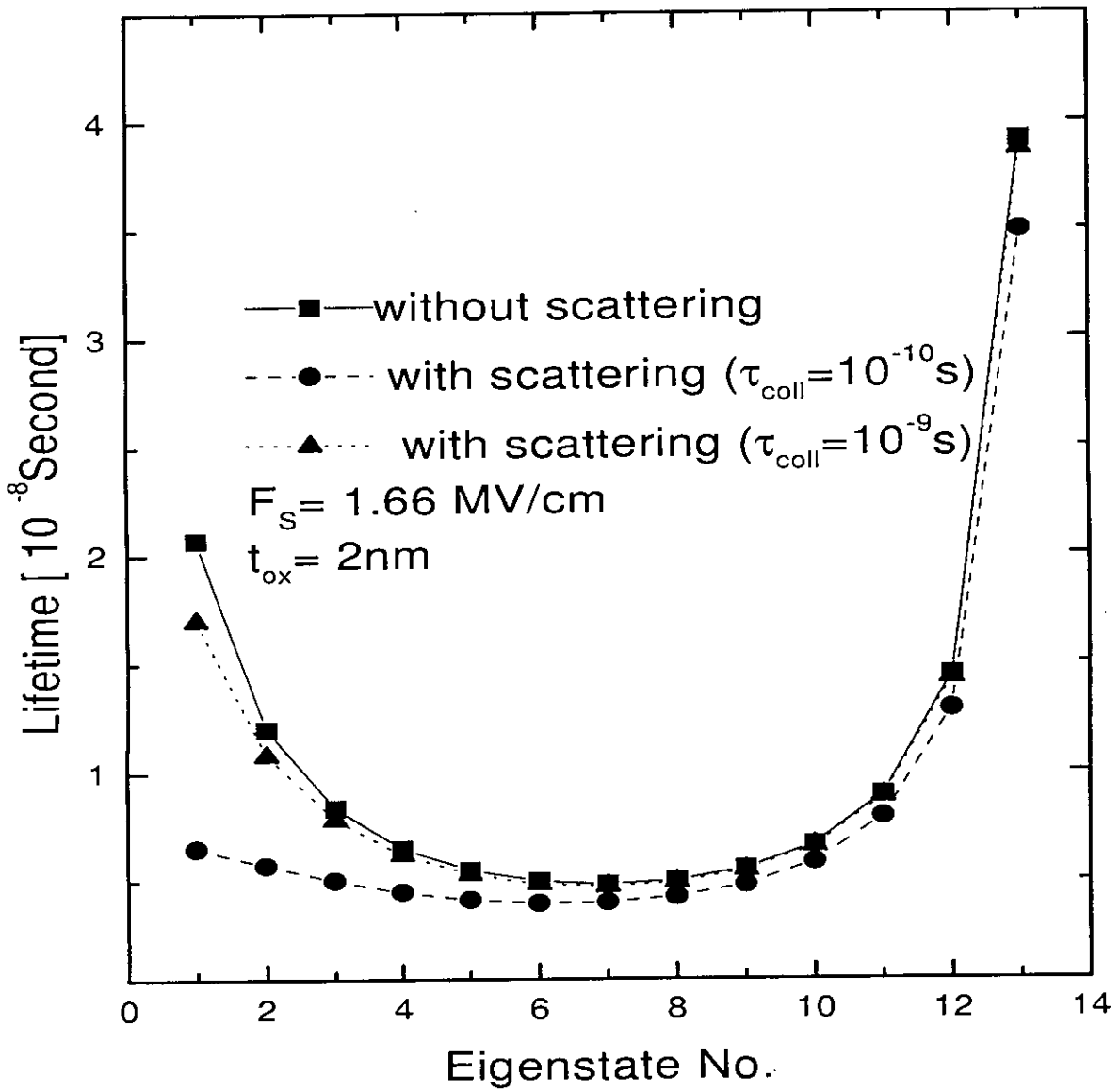


Fig. 5.4: Variation of lifetimes of different eigenstates for two different values of collision time and two different collision time profile with $F_s = 1.66 \text{ MV/cm}$ and $t_{\text{ox}} = 2 \text{ nm}$.

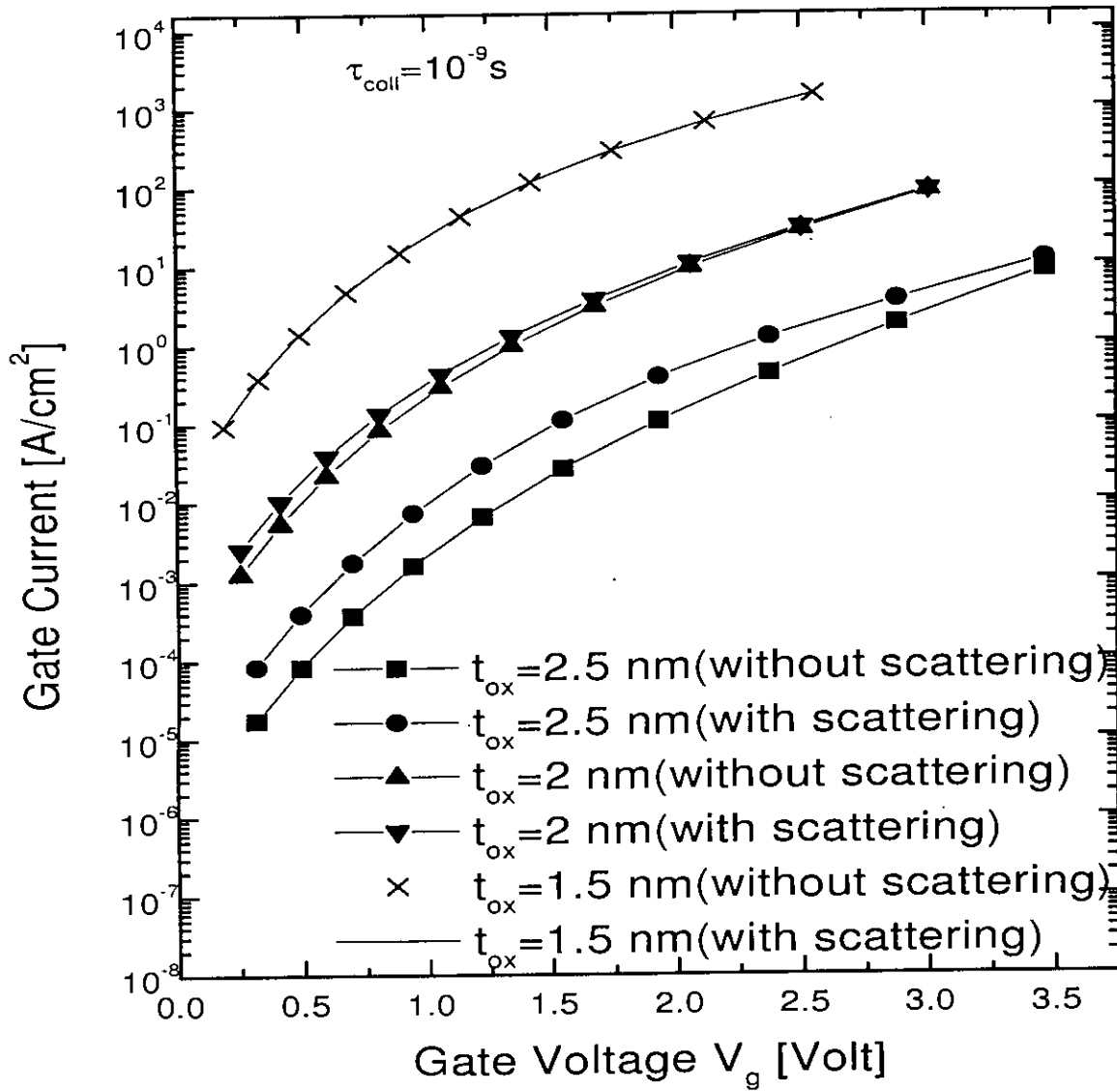


Fig. 5.5: Variation total gate current with gate voltage with and without phase-breaking scattering for three t_{ox} , for constant $\tau_{coll} = 10^{-9} \text{ s}$.

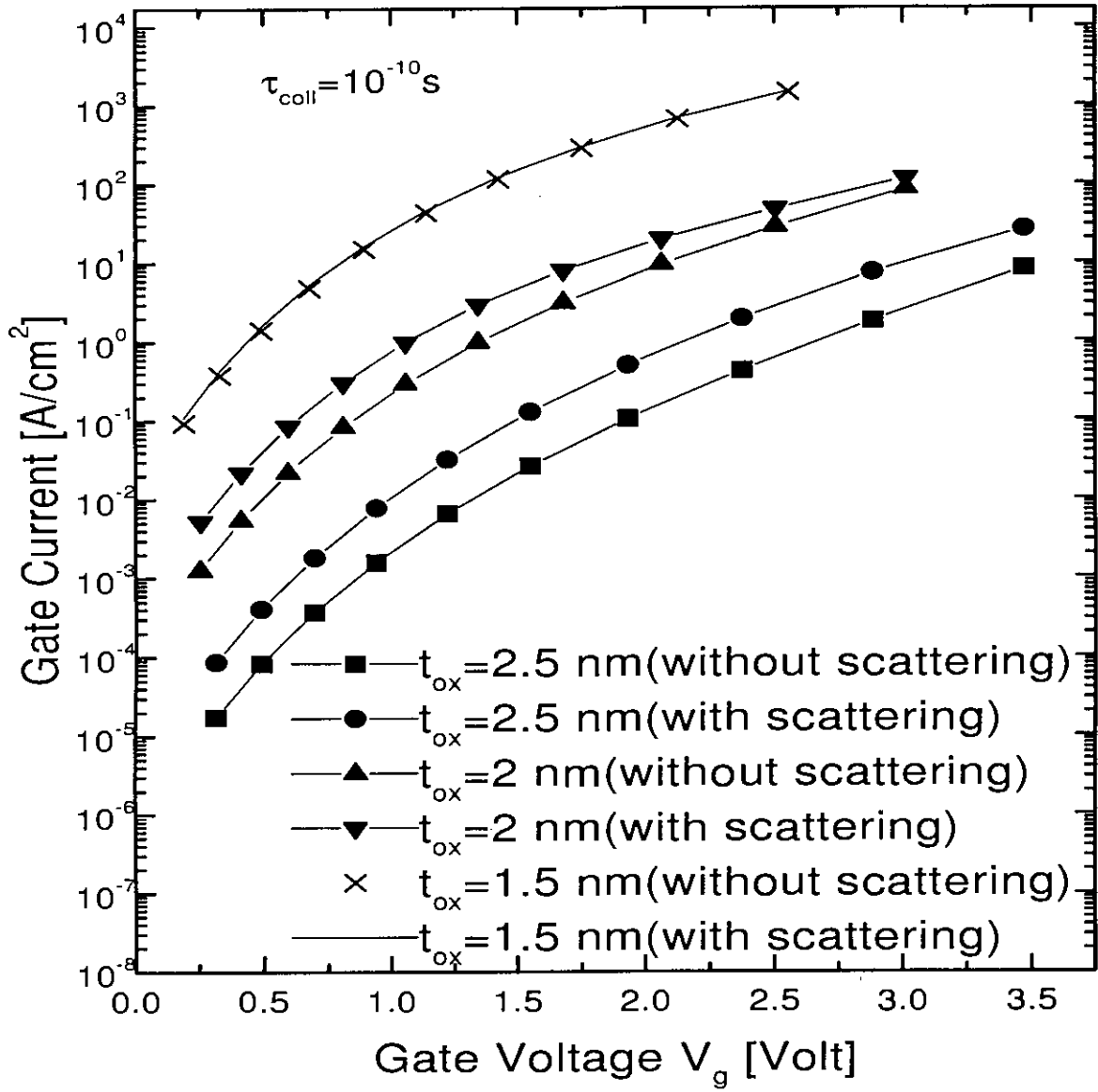


Fig. 5.6: Variation total gate current with gate voltage with and without phase-breaking scattering for three t_{ox} , for constant $\tau_{coll} = 10^{-10} \text{ s}$.

the discrepancies between experimental and simulated direct tunneling currents reported in [18, 19, 22]. In these studies it was seen that although the simulated currents agreed well with experimental values in thin gate oxide devices ($t_{ox} < 1.8$ nm), in devices with $t_{ox} \geq 2$ nm, especially at lower gate voltages, the experimentally measured gate current was higher than the simulated one when effects of scattering were not included. Thus, the results of the present study provide an explanation for the difference between experimental and existing simulated results and demonstrate the need for incorporating phase-breaking scattering effects for accurate simulation of direct tunneling gate current.

Chapter 6

Conclusion

The direct tunneling gate current of a deep submicron MOSFET flows due to Quantum Mechanical tunneling of inversion layer carriers from semiconductor to the gate electrode. The value of direct tunneling current is influenced by the presence of inelastic or phase-breaking scattering caused by phonons, defects, interface states and impurities in the oxide.

6.1 Summary

A new technique is presented to calculate the direct tunneling gate current in deep submicron MOSFETs. In this technique, the effects of wave function penetration on self consistent potential profile can be incorporated. The method is numerically simple and does not require either lengthy matrix manipulation or calculation of complex eigenenergies. An attractive feature of this technique is that electron inelastic scattering effects on tunneling current can be included in the modeling. The eigenenergies and the lifetimes of the quasi-bound states are calculated from the peaks and the broadening of the 1D DOS around each eigenenergy. It is seen that the lifetimes are sensitive to the changes in either the surface electric field or the oxide width. The contribution to the direct tunneling current comes dominantly from the lowest eigenstate. Scattering effects are found to be more significant in devices with thicker oxides at lower gate voltages. Scattering also has non-trivial effects on the lifetimes of the inversion layer states. Numerical calculations of direct tunneling current are presented. Results show that inclusion of inelastic scattering can explain the observed mismatch between experimental and simulated tunneling currents in the literature at low gate

voltages that did not take into account inelastic scattering effects.

The present study suffers from certain limitation, such as, lacking self-consistent calculation of potential profile, using simple and incomplete model for collision time and calculation of current for only certain condition of device.

6.2 Suggestions for Further Work

The self-consistent calculation of carrier concentration for determining the potential profile involves coupled solution of Schrödinger's and Poisson's equations. The self-consistent potential profile will result in a closer match between the simulated current and the measured one. In the present work, in order to avoid numerical complexity, potential profile has not been calculated in a self-consistent manner. But it leaves the scope of incorporating self-consistency in the calculations.

A thorough study demands the calculation to be made in different device conditions. The current calculated in this work is for no signal condition and after inversion has occurred. But calculation may be done for weak inversion, as well as, for accumulation.

Accurate modeling of inelastic scattering considering actual collision process should be made. This requires proper determination of energy and position dependence of collision time. The inelastic scattering phenomena includes phase change, as well as, energy change of tunneling electrons colliding with phonons, defects, interface states or impurities. Although, for simplifying the calculation, the energy change of the scattered electrons has been ignored in the present work, its inclusion will increase the accuracy of the calculation.

Bibliography

- [1] "The National Technology Roadmap for Semiconductors: Technology Needs," Semiconductor Industry Association, San Jose, California, 1997.
- [2] S. M. Sze, *Physics of Semiconductor Devices*, Second edition, Wiley Eastern Limited, pp. 362-366, 1987.
- [3] Y. Tsvividis, *Operation and Modeling of the MOS Transistor*, McGraw-Hill, Ch. 2, 1999.
- [4] F. Stern, "Self-consistent results for n-type Si inversion layers," *Physical Review B*, vol. 5, pp. 4891-4899, 1972.
- [5] C. Moglestue, "Self-consistent calculation of electron and hole inversion charges at silicon-silicon dioxide interfaces," *J. Appl. Phys.*, vol. 59, pp. 3175-3183, 1986.
- [6] M. J. Van Dort, P. H. Woerlee, A. J. Walker, "A simple model for quantization effects in heavily-doped silicon MOSFETs at inversion conditions," *Solid-State Electron.*, vol. 37, pp. 411-414, 1994.
- [7] Scott A. Hareland, Shyam Krishnamurthy, Srinivas jallepali, Choh-Fei Yeap, Khaled Hasnat, Al F. Tasch, Christine M. Mazier, "A Computationally efficient model for inversion layer quantization effects in deep submicron n-channel MOSFET's," *IEEE Trans. on Electron Devices*, vol. 43, pp. 90-95, 1996.
- [8] G. Paasch, S. Scheinert, K. Tarnay, "Influence of inversion channel quantisation on the surface potential in the MOS structure," *Phys. Stat. Sol.*, vol. 149, pp. 751-755, 1995.

- [9] S. Takagi and A. Toriumi, "Quantitative understanding of inversion-layer capacitance in Si-MOSFETs," *IEEE Trans. on Electron Devices*, vol. 42, pp. 2125-2130, 1995.
- [10] S. Takagi, M. Takayanagi and A. Toriumi, "Characterization of inversion-layer capacitance of holes in Si MOSFET's," *IEEE Trans. on Electron Devices*, vol. 46, pp. 1446-1450, 1999.
- [11] S. Jallepalli, J. Bude, W.-K. Shih, M. R. Pinto, C. M. Maziar and A. F. Tasch, "Electron and hole quantization and their impact on deep submicron silicon p- and n-MOSFET characteristics," *IEEE Trans. on Electron Devices*, vol. 44, pp. 297-302, 1997.
- [12] C. A. Ritcher, A. R. Hefner, E. M. Vogel, "A comparison of quantum mechanical capacitance-voltage simulators," *IEEE Electron Device Letters*, vol. 22, pp. 35-37, 2001.
- [13] M. Giannini, A. Pacelli, A. L. Lacaita, L. M. Perron, "Effect of oxide tunneling on the measurement of MOS interface states," *IEEE Electron Device Letters*, vol. 21, pp. 405-407, 2000.
- [14] A. Pacelli, A. S. Spinelli and L. M. Perron, "Carrier quantization at flat bands in MOS devices," *IEEE Trans. on Electron Devices*, vol. 46, pp. 383-387, 1999.
- [15] Douglas W. Barlage, James T. O'Keeffe, J. T. Kavalieros, M. M. Nguyen, R. S. Chau, "Inversion MOS capacitance extraction for high-leakage dielectrics using a transmission line equivalent circuit," *IEEE Electron Device letters*, vol. 21, pp. 454-456, 2000.
- [16] C. Fiegna and A. Abramo, "Analysis of quantum effects in nonuniformly doped MOS structures," *IEEE Trans. on Electron Devices*, vol. 45, pp. 877-880, 1998.
- [17] Farhan Rana, Sandip Tiwari, D. A. Buchanan, "Self consistent modeling of accumulation layers and tunneling currents through very thin oxides," *Appl. Phys Lett*, vol. 69, pp. 1104-1106, 1996.

- [18] S. H. Lo, D. A. Buchanan, Y. Taur, W. Wang, "Quantum-mechanical modeling of electron tunneling current from the inversion layer of ultra-thin-oxide nMOSFET's," *IEEE Electron Device Letters*, vol. 18, pp. 209-211, 1997.
- [19] Yuan Taur, "The incredible shrinking transistor," *IEEE Spectrum*, vol. 36, pp. 25-29, 1999.
- [20] W-K Shih, E. X. Wang, S. Jallepalli, F. Leon, C. M. Maziar and A. F. Tasch, "Modeling gate leakage current in nMOS structures due to tunneling through an ultra-thin oxide," *Solid-State Electron.*, vol. 42, pp. 997-1006, 1998.
- [21] Leonard F. Register, Elyse Roesenbaum, Kevin Yang, "Analytical model for direct tunneling current in polysilicon-gate-metal-oxide-semiconductor devices," *Appl. Phys Lett*, vol. 74, pp. 457-459, 1999.
- [22] Nian Yang, W. Kirklel Henson, John R. Hauser, J. J. Wortman, "Modeling study of ultrathin gate oxide using direct tunneling current and capacitance-voltage measurements in MOS devices," *IEEE Trans. on Electron Devices*, vol. 46, pp. 292-294, 1999.
- [23] Sivkumar Mudanai, Yang-Yu Fan, Qiqing (Christine) Ouyang, Al F. Tasch, Sanjay Kumar Banerjee, "Modeling of direct tunneling through gate dielectric stacks," *IEEE Trans. on Electron Devices*, vol. 47, pp. 1851-1857, 2000.
- [24] Yee Chia Yeo, Qiang Lu, Wen Chin Lee, Tsu-Jae King, Chenming Hu, Xiewen Wang, Xin Guo, T. P. Ma, "Direct unneling gate leakage current in transistors with ultra thin silicon nitride gate dielectrics," *IEEE Electron Device Letters*, vol. 21, pp 540-542, 2000.
- [25] A. Haque, A. Rahman, I. B. Chowdhury, "On the use of appropriate boundary conditions to calculate the normalized wave functions in the inversion layers of MOSFETs with ultra-thin gate oxides," *Solid-State Electron.*, vol. 44, pp. 1833-1836, 2000.

- [25] K. Sakakibara *et al.*, "A quantitative analysis of time-decaying reproducible stress-induced leakage current in SiO_2 film," IEEE Trans. on Electron Devices, vol. 44, pp. 1002-1007, 1997.
- [26] S. Tagaki, N. Yasuda, A. Toriumi, "Experimental evidence of inelastic tunneling and new I-V model for stress-induced leakage current," in IEDM Tech. Dig., pp. 323-326, 1996.
- [27] C. T. Liu *et al.*, "Intrinsic and stress-induced traps in the direct tunneling current 2.3-3.8 nm oxides and unified characterization methodologies of sub 3 nm oxides," in IEDM Tech. Dig., pp. 85-88, 1997.
- [28] J. Wu, L.F. Register, and E. Rosenbaum, "Trap-assisted tunneling current through ultra-thin oxide," in TRPS Tech. Dig., pp. 396-399, 1999
- [29] L. Larcher, A. Paccagnella and G. Ghidini, "A model of the stress-induced leakage current in gate oxides," IEEE Trans. on Electron Devices, vol. 48, pp. 285-288, 2001.
- [30] A. N. Khondker, M.R. Khan and A.F.M. Anwar, "Transmission line analogy of resonance tunneling phenomena: the generalized impedance concept," J. Appl. Phys., vol. 63, pp. 5191-5193, 1988.
- [31] Simon Ramo, John R. Whinnery, Theodore Van Duzer, *Field and Waves in Communication Electronics*, John Wiley Sons, pp. 23-28, 1965.
- [32] A. Haque and A. N. Khondker, "An efficient technique to calculate the normalized wave functions in arbitrary one-dimensional quantum well structures," J. Appl. Phys., vol. 84, pp. 5802-5804, 1998.
- [33] A. Rahman and A. Haque, "A study into the broadening of quantized inversion layer states in deep submicron MOSFETs," Solid-State Electron., to be published, 2001.
- [34] Shin-ichi Tagaki, Mariko Takayanag, Akira Toriumi, "Impact of electron and hole inversion-layer capacitance on low voltage operation of scaled n- and p-MOSFET's," IEEE Trans. on Electron Devices, vol. 47, pp. 999-1005, 2000.

- [35] A. Douglas Stone and P. A. Lee, "Effects of inelastic processes on resonant tunneling in one dimension," Physical Review Letters, vol. 54, pp. 1196-1199, 1985.
- [36] G. Innaccone and B. Pellegrini, "Compact formula for density of states in a quantum well," Physical Review B, vol. 53, pp. 2020-2025, 1995.
- [37] A. N. Khondker and Muhammad A. Alam, "Buttiker-Landauer conductance formulas in the presence of inelastic scattering," Physical Review B, vol. 44, pp. 5444-5452, 1991.
- [38] Quazi Deen Mohd Khoshru, "Investigation on hot-hole induced degradation of MOS devices," PhD dissertation, Osaka University, Japan, 1994.

